Dyes with Segmental Mobility: Molecular Rotors

Mark A. Haidekker, Matthew Nipper, Adnan Mustafic, Darcy Lichlyter, Marianna Dakanali, and Emmanuel A. Theodorakis

Abstract Molecular rotors are fluorescent molecules that are characterized by the ability to form twisted states through the rotation of one segment of the structure with respect to the rest of the molecule. Intramolecular rotation changes the ground-state and excited-state energies, and molecular rotors deexcite from the twisted state either without photon emission or with a different wavelength than from the LE state. Intramolecular rotation is strongly dependent on the solvent. Solvent polarity, hydrogen bond formation, isomerization, excimer formation, and steric hindrance are predominant forms of solvent–fluorophore interaction. Of highest importance is steric hindrance, because it links the solvent's microviscosity to the formation rate of TICT states, which, in turn, determines the spectral emission. For this reason, molecular rotors have found a wide range of applications as fluorescent sensors of microviscosity and solvent free volume. Application examples include bulk viscosity measurement, probing dynamics of polymer formation, protein sensing and probing of protein aggregation, and microviscosity probing in living cells.

Keywords Biofluids · Chemosensors · Emission spectroscopy · Mechanosensors · Optical properties · Polarity · Rheology · Twisted intramolecular charge transfer · Viscosity

Contents

M.A. Haidekker (✉), M. Nipper, A. Mustafic, and D. Lichlyter
University of Georgia, Athens, GA 30602, USA
e-mail: mhaidekk@uga.edu

M. Dakanali and E.A. Theodorakis
Department of Chemistry and Biochemistry, University of California, San Diego, La Jolla, CA 92093-0358, USA

A.P. Demchenko (ed.), *Advanced Fluorescence Reporters in Chemistry and Biology I: Fundamentals and Molecular Design*, Springer Ser Fluoresc (2010) 8: 267–308,
DOI 10.1007/978-3-642-04702-2_8,

1 Introduction

The term *molecular rotor* refers to a group of fluorescent molecules with an intramolecular charge transfer (ICT) mechanism, which undergo a twisting motion in the excited state. This family of fluorophores is often known as twisted intramolecular charge transfer (TICT) complexes. After photon absorption, a molecular rotor can return to the ground state either from the locally excited (LE) state or from the twisted state. The energy gaps between the LE and twisted states to the ground state are very different, and the deexcitation from the twisted state has either a red-shifted emission wavelength or no emission at all. One of the main reasons why molecular rotors are intensively investigated is the dependency of the twisted-state deexcitation rate on the local environment, namely on the solvent's microviscosity and polarity.

The anomalous dual fluorescence emission of *p-N,N*-dimethylamino benzonitrile (DMABN) in polar solvents was first reported by Ernst Lippert in 1962. Emission spectra of DMABN in solvents of different polarity show a dual emission, where the red-shifted emission is stronger relative to the primary emission when the solvent polarity increases. Furthermore, it can be observed that overall emission intensity is reduced in more polar solvents, but higher solvent viscosity increases the emission intensity. Spectra of DMABN in different solvents are shown in the chapter of Tomin in this book [1].

Molecular rotors have in common that fluorescent excitation leads to an ICT, in the case of DMABN from the nitrogen in the dimethylamino electron donor group to the nitrile electron acceptor group (Fig. 1). The ICT leads to a highly polar

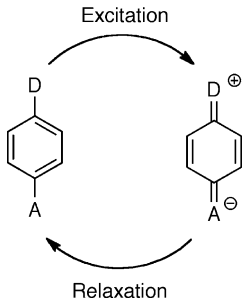

Fig. 1 Mesomeric structures of a *para*-substituted benzene intramolecular charge transfer (ICT) complex in the ground state and in the dipolar excited state

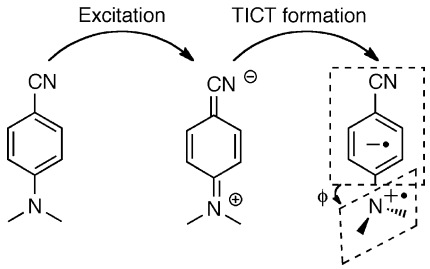

Fig. 2 Intramolecular twisting in DMABN. In the excited state, the molecule has a high propensity to rotate the dimethylamino group out of the planar ground-state configuration [3]. This process changes the dipole energy, and relaxation from the twisted state causes the red-shifted emission band

structure in the excited state. The TICT hypothesis was first formulated by Rotkiewicz et al. [2] whereby the molecule can undergo an intramolecular twisting motion around a single bond. Twisted-state formation of DMABN is sketched in Fig. 2. Deexcitation of the molecule can occur either from the planar LE state or from the twisted state, and both cases lead to different deexcitation energies. In the case of DMABN, the red-shifted emission band can be explained by a deexcitation from the lower-energy twisted state.

Twisted-state formation is strongly influenced by the surrounding media. Steric hindrance can reduce the formation of twisted states, and polar solvents show reorientation around the charged dipole and may even form hydrogen bonds with the fluorophore. The ability to respond to multiple solvent effects makes customization of these fluorophores possible. Different TICT-forming fluorophores can be used for monitoring photochemical effects, quenching, and competitively coupled and consecutively coupled product species [4]. A common example of a competitive scheme can be found in the stilbene group. Stilbenes can form nonradiative secondary products in direct competition with the formation of radiative products. If the reaction dynamics are favorable for the formation of nonradiative products, intramolecular fluorescence quenching takes place [5], evidenced by a lower quantum yield. These examples demonstrate how the twisted-state mechanism can form the basis for the unique sensitivity of molecular rotors toward the solvent. There are several mechanisms through which the solvent influences the fluorescent properties of a TICT molecule. Of highest relevance are excimer formation, isomerization, polar reorientation of the solvent molecules, and steric hindrance of intramolecular rotation by the solvent. This chapter focuses on solvent interaction through steric hindrance. An overview of the interaction mechanisms of TICT fluorophores with the solvent, an overview of commonly used families of TICT-forming molecules, and practical applications of TICT complexes for sensing solvent properties are given in this chapter.

2 Photophysical Properties of Molecular Rotors

Two phenomena need to be examined to understand the interaction of a molecular rotor with its environment. First, changes of the ground-state and excited-state energies between LE and twisted states need to be examined, and second, the

interaction of the fluorophore in its excited state with the solvent needs to be considered.

In most fluorescent processes, the lowest unoccupied molecular orbital (LUMO) and the highest occupied molecular orbital (HOMO) are the two relevant levels considered in electron energy change. HOMO–LUMO photoexcitation of a fluorophore promotes one of the two present electrons to an antibonding state that is usually denoted by *. In addition to the σ and π orbitals (a typical fluorescence-related transition is π–π^*), electrons can also be promoted from nonbonding electrons such as those that surround oxygen or nitrogen. These *n*-electrons can move to either the σ^* or π^* antibonding state. ICT complexes are characterized by the presence of electron donor and acceptor groups that are connected via a π-conjugation system. The donor group usually provides *n*-electrons. The π-conjugation allows interaction between the donor and acceptor groups so that the nonbonding electrons of the donor can be delocalized to the unoccupied orbitals of the acceptor. A key component is the spatial separation of the donor and acceptor groups with the π-system so that the orbitals of the donor and acceptor groups have negligible spatial overlap.

The promotion to a higher energy level can cause the electron to relax to a number of vibrational states before the molecule's return to the ground state and consequential photon release. This relaxation is the energy loss that is predominantly responsible for the wavelength shift between absorption and fluorescence (Stokes shift). In TICT complexes, the formation of the twisted state can be interpreted as a dominant vibrational state that leads to major energy loss. The twisting of the molecule is a result of an unbalanced dipole moment upon photon absorption and requires the ability of the nitrogen atom in the donor group to undergo a change from a pyramidal configuration in the ground state to a planar configuration in the charge transfer state [6]. A qualitative sketch of the energy levels of a TICT molecule can be seen in Fig. 3 [7–9]. The ground-state energy level

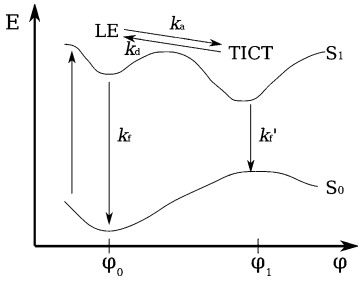

Fig. 3 Ground-state and excited-state energies in the planar and twisted configurations of a TICT molecule. Photon absorption usually elevates the molecule to the LE state in the planar configuration, where the angle of intramolecular rotation, φ_0, is close to zero. From the LE state, the molecule can return to the ground state with a rate k_f, or it undergoes intramolecular rotation with a rate k_a. The twisted state is characterized by a larger intramolecular rotation angle φ_1, usually 90°. From the twisted state, the molecule can return to the ground state with a rate k_f' or it returns to the LE state. The return rate to the LE state, k_d, is usually very small, but can be increased in nonpolar solvents

is higher in the twisted configuration, and the molecule has a natural tendency to return to the planar state. The excited-level TICT state has a lower energy than the LE state, but the states are separated by a small energy maximum that needs to be overcome when the molecule enters the TICT state from the LE state. It has also been found that any effects that delay the planar formation, i.e., placing the amino group within a heterocyclic ring [6], lead to an overall increase in the energy barrier between LE and TICT states. The energy barrier between the LE and TICT states is solvent-dependent. For DMABN, a polar solvent lowers the barrier, and viscous solvents generally elevate the barrier [9]. Consequently, the conversion rates are solvent-dependent. The fluorescent lifetimes $\tau_f = k_f^{-1}$ and $\tau_f' = k_f'^{-1}$ have been determined to be near 2.5–3 ns. The TICT formation rate k_a is in the order of 10^{10} s^{-1}, and the return rate k_d is strongly solvent-dependent and has been found to vary in magnitude from 10^8 to 10^{10} s^{-1} [10, 11]. Since these rates are highly dependent on the dye and the solvent, the values are given for orientation only. The actual rotational motion takes place within less than 20 ps.

From the excited-state conversion rates (k_a and k_d), it is possible to calculate the ratio of the quantum yields between emission from the twisted and LE states. The ratio of the steady-state quantum yields from the locally excited state ϕ_{LE} and the TICT state ϕ_{TICT} for DMABN and other aminobenzonitrile derivatives is described in (1) [12],

$$\frac{\phi_{\text{TICT}}}{\phi_{\text{LE}}} = \frac{k_f'}{k_f} \cdot \frac{k_a}{k_d + 1/\tau_{\text{CT}}'} \tag{1}$$

where τ_{CT}' is the TICT lifetime, k_f' is the deexcitation rate from the twisted state, k_f is the deexcitation rate from the LE state, k_a is the rate of TICT formation from the LE state, and k_d is the reverse rate, i.e., the return rate to the LE state from the TICT state. Generally, $k_a \gg k_d$ so that relaxation from the TICT state dominates. Molecular rotors that have radiationless deexcitation from the TICT state exhibit a low quantum yield from a single (LE) emission band.

Two examples for the energy levels of the S_0 and S_1 states in dependency of the intramolecular rotation angle were obtained through computational methods by Stsiapura et al. [13] and Allen et al. [14] for thioflavin T and 9-(dicyanovinyl)-julolidine (DCVJ), two molecules known for their ability to form TICT states. The energy levels are shown in Fig. 4 to provide quantitative data that relate to Fig. 3. In the ground state, the molecule tries to find the energy-minimizing conformation. In the case of DCVJ, the minimum energy exists when the molecule is fully planar. Thioflavin T prefers a 37° twist angle as the energy-minimizing configuration. In a similar manner, the molecules rapidly assume their minimum-energy configuration in the excited state by performing an intramolecular rotation. In both thioflavin T and DCVJ, the minimum excited-state energy is reached when the donor and acceptor planes are rotated 90° relative to each other. Excited-state intramolecular rotation takes place very rapidly, typically in the low picosecond range, when the rotation is not hindered by the solvent. When the energy gaps between S_1 and S_0

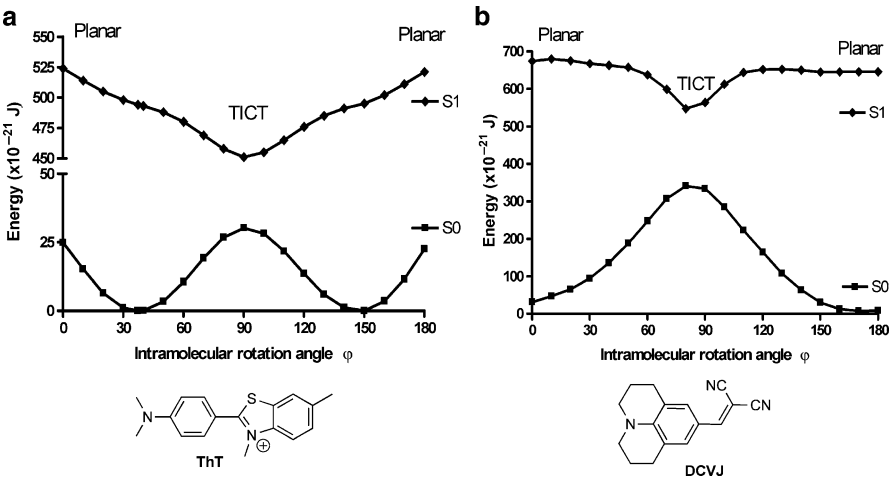

Fig. 4 Ground-state and excited-state energies of the TICT complexes thioflavin T (a) and 9-(dicyanovinyl)-julolidine (DCVJ) (b) as a function of the intramolecular rotation angle (data from Stsiapura et al. [13] and Allen et al. [14]). In both cases, energy levels were determined by quantum mechanical simulations. For thioflavin T, the energy difference between S_1 and S_0 corresponds to approximately 400 nm in the planar state and 470 nm in the twisted state. In the case of DCVJ, the energy differences correspond to 310 and 960 nm, respectively. The DCVJ energy levels reflect a rotation around the vinyl double bond

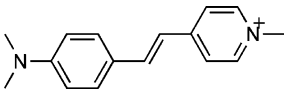

Fig. 5 Structure of *p*-(dimethylamino) stilbazolium (*p*-DASPMI)

states between the planar and TICT configurations are relatively small, dual-band emission occurs. An example is DMABN where the energy gap between the S_1 and S_0 states is about 30% smaller in the TICT state than in the planar state. With a larger donor–acceptor distance, the energy gap between S_1 and S_0 states becomes dramatically smaller in the TICT configuration than in the planar configuration. When returning to the ground state from the TICT state, many molecular rotors cross an energy gap that is so low that photon emission cannot be detected [15]. The TICT-forming dye *p*-(dimethylamino)stilbazolium (*p*-DASPMI, Fig. 5) was found to have an energy gap of 3 eV (corresponding to 412 nm) in the planar configuration and approximately 1.2 eV (corresponding to 1,030 nm) after a 90° twist around the central double bond, and relaxation from this twisted state is considered radiationless [16]. The molecular rotor DCVJ (Fig. 4b) was found to have an energy gap more than three times larger in the planar configuration than in the TICT configuration [14]. In the extreme case, the energy gap can actually become negative [17]. The computational models that were used to compute the energy gaps did not

consider solvent influences, and the actual spectra show a peak emission at higher wavelengths than the wavelengths that correspond to the energy gaps. DCVJ, for example, has a peak emission near 500 nm, whereas the planar-state energy gap (Fig. 4b) corresponds to 310 nm. A molecular rotor with radiationless relaxation from the twisted state exhibits only a single emission band, but its quantum yield is highly dependent on the environment. It is therefore important to distinguish between molecular rotors that have solvent-dependent dual emission bands and those that have a single emission band with a solvent-dependent quantum yield. The latter group is particularly interesting, because some representatives show a good separation between the influence of polarity and viscosity [14, 18, 19]. Popular examples are the julolidine-based dyes, among them DCVJ (Fig. 4). Radiationless relaxation from the TICT state occurs because of the low TICT $S_1 - S_0$ energy gap. The LE state has a relatively low dipole moment and shows only a minimal solvatochromic shift. Solvent microviscosity strongly influences TICT formation rate and therefore the quantum yield of LE emission. Consequently, the emission wavelength is weakly polarity-dependent, whereas the quantum yield is almost exclusively determined by solvent viscosity [14, 18, 19].

The predominant mechanisms of the interaction between TICT molecules and the solvent deserve further explanation. TICT fluorophores are known to be sensitive to solvent polarity. DMABN with its red-shifted second emission band is a particularly well-researched example. Any ICT complex has an increased dipole moment in the excited state compared to the ground state because of the photoinduced charge separation. In the example of DMABN, the ground-state dipole moment is approximately 6 D (1 D (Debye) $\approx 3.33564 \times 10^{-23}$ C m), and the excited-state dipole moments are approximately 12 D in the LE state and 15 D in the TICT state. Polar solvent molecules orient themselves along the fluorophore dipole by aligning their electric fields. Upon relaxation, the solvent molecules return to the ground-state orientation. As a consequence, the fluorophore exhibits a bathochromic shift that reflects the energy expended for the reorientation of the solvent molecules. The magnitude of this effect depends on the solvent polarity, that is, its dielectric constant ε. In addition, solvent polarity directly influences the TICT formation rate k_a and the reverse rate k_d in a manner that emission from the TICT states increases in more polar solvents [12]. It is possible to design the chemical structure of TICT molecules such that the ratio between intrinsic dual-band fluorescence and outside polar effects can be optimized [4].

The polarity of a molecule is often closely correlated with the ability to form hydrogen bonds with solvent molecules that are in close proximity to the fluorophore. Hydrogen bond formation can lead to spectral shifts as well as changes in the ordering of states. State change ordering occurs in heterocycles and carbonyl compounds, which results in a lower energy difference between the lowest ($n \rightarrow \pi^*$) and ($\pi \rightarrow \pi^*$) singlet states as a consequence of ground-state hydrogen bonding [20–22]. Hydrogen bonds also have a propensity to alter intermolecular charge transfer rates of TICT molecules and, in turn, increase the TICT formation rate of the fluorophore [21]. Therefore, hydrogen bond formation has similar effects on the fluorescent emission as polar–polar interaction.

One of the most popular applications of molecular rotors is the quantitative determination of solvent viscosity (for some examples, see references [18, 23–27] and Sect. 5). Viscosity refers to a bulk property, but molecular rotors change their behavior under the influence of the solvent on the molecular scale. Most commonly, the diffusivity of a fluorophore is related to bulk viscosity through the Debye–Stokes–Einstein relationship where the diffusion constant D is inversely proportional to bulk viscosity η. Established techniques such as fluorescent recovery after photobleaching (FRAP) and fluorescence anisotropy build on the diffusivity of a fluorophore. However, the relationship between diffusivity on a molecular scale and bulk viscosity is always an approximation, because it does not consider molecular-scale effects such as size differences between fluorophore and solvent, electrostatic interactions, hydrogen bond formation, or a possible anisotropy of the environment. Nonetheless, approaches exist to resolve this conflict between bulk viscosity and apparent microviscosity at the molecular scale. Förster and Hoffmann examined some triphenylamine dyes with TICT characteristics. These dyes are characterized by radiationless relaxation from the TICT state. Förster and Hoffmann found a power–law relationship between quantum yield and solvent viscosity both analytically and experimentally [28]. For a quantitative derivation of the power–law relationship, Förster and Hoffmann define the solvent's microfriction κ by applying the Debye–Stokes–Einstein diffusion model (2)

$$\kappa = 8\pi r^3 \eta \tag{2}$$

where η is the dynamic bulk viscosity of the solvent and r is the effective radius of one phenyl group of the triphenylamine dye. Förster and Hoffmann interpret the three arms of the dye as rotational masses that obey the classical differential equation of rotation, where the constant for the first-order term is the electrostatic force that returns the phenyl groups to their initial angle. Three special cases emerge from this approach. First, when the solvent viscosity is very low, the fluorescence quantum yield reaches a minimum that is solvent-independent. Second, in the range of extremely high viscosities, radiative deexcitation dominates with a negligible rotational deexcitation rate, and the quantum yield follows (3),

$$\phi_F \approx \frac{\tau_s}{\tau_0}\left(1 - \frac{6\sigma^2}{\eta^2}\right) \tag{3}$$

where σ is a dye-dependent constant that contains all dye-specific and viscosity-independent variables, τ_0 is the natural lifetime (i.e., the lifetime in the absence of any nonradiative relaxation events), and τ_s is the lifetime in the absence of all deactivation processes through conformational changes. The dye-dependent constant σ has units of viscosity. Under the assumption of the size of a phenyl group of $r \approx 2 \times 10^{-10}$ m and the energy resulting from the potential differences $\alpha \approx 10^{-9}$ J, a typical value for this constant is $\sigma = 100$ Pa s [28]. It can be seen that the limiting case of (3) for $\eta \gg \sigma$ yields the maximum achievable quantum

yield of $\phi_F \approx \tau_s/\tau_0$. The third and most important case is obtained for intermediate viscosity values when $\eta \ll \sigma$ and the quantum yield obeys (4):

$$\phi_F \approx 0.893 \cdot \frac{\tau_s}{\tau_0} \left(\frac{\eta}{\sigma}\right)^{2/3} \tag{4}$$

Most of the constants in (4) are dye-dependent constants that can be determined experimentally. It is therefore straightforward to combine those constants into a single dye-dependent constant C and rewrite (4) as (5),

$$\phi_F = C \cdot \eta^x \tag{5}$$

which is the empirical form of the relationship between viscosity and quantum yield most often referred to as the Förster–Hoffmann equation. In (5), all variables are assumed as unitless (in fact, C has units of viscosity to the power of $-x$ as evident from (4)). The special case of $x = 2/3$ emerges from an integration step that leads to (4). It can be interpreted as a maximum value when $\eta \ll \sigma$, and experimental results may yield lower values of x.

Loutfy and coworkers [29, 30] assumed a different mechanism of interaction between the molecular rotor molecule and the surrounding solvent. The basic assumption was a proportionality of the diffusion constant D of the rotor in a solvent and the rotational reorientation rate k_{or}. Deviations from the Debye–Stokes–Einstein hydrodynamic model were observed, and Loutfy and Arnold [29] found that the reorientation rate followed a behavior analogous to the Gierer–Wirtz model [31]. The Gierer–Wirtz model considers molecular free volume and leads to a power–law relationship between the reorientation rate and viscosity. The molecular free volume can be envisioned as the void space between the packed solvent molecules, and Doolittle found an empirical relationship between free volume and viscosity [32] (6),

$$\eta = A \cdot \exp\left(B \frac{V_0}{V_f}\right) \tag{6}$$

where A and B are solvent-specific empirical constants, V_f is the fluid free volume, and V_0 is the van der Waals volume of the fluorescent dye. Loutfy and Arnold [29] showed experimentally that the nonradiative decay rate (i.e., the intramolecular rotation rate) behaves in an analogous manner, and that the nonradiative decay rate can be described in terms of free volume through (7) [30],

$$k_{nr} = k_{nr}^0 \exp\left(-x' \frac{V_0}{V_f}\right) \tag{7}$$

where k_{nr}^0 is an intrinsic, solvent-independent relaxation rate, and x' is a solvent-dependent constant.

Substitution of the exponential term from (6) into (7) replaces the free-volume term by the solvent viscosity and provides an equation for the viscosity-dependent nonradiative decay rate, from which the quantum yield emerges (8):

$$\phi_F \approx \frac{k_r}{k_{nr}^0} \cdot \left(\frac{\eta}{A}\right)^x \tag{8}$$

In (8), the solvent-independent constants k_r, k_{nr}^0, and A^x can be combined into a common dye-dependent constant C, which leads directly to (5). The radiative decay rate τ_r can be determined when rotational reorientation is almost completely inhibited, that is, by embedding the molecular rotor molecules in a glass-like polymer and performing time-resolved spectroscopy measurements at 77 K. In one study [33], the radiative decay rate was found to be $k_r = 2.78 \times 10^8\ \mathrm{s}^{-1}$, which leads to the natural lifetime $\tau_0 = 3.6$ ns. Two related studies where similar fluorophores were examined yielded values of $\tau_0 = 3.3$ ns [25] and $\tau_0 = 3.6$ ns [29]. It is likely that values between 3 and 4 ns for τ_0 are typical for molecular rotors.

Contrary to the derivation proposed by Förster and Hoffmann where the value of the exponent x was specified to be rigidly 2/3 as the result of an integration, Loutfy and coworkers allow for a variable value of x that depends both on the dye and the solvent. Since the parameter A that originates from (6) is also solvent-dependent, the power–law relationship between viscosity and quantum yield needs calibration for any dye–solvent combination before the measurement of bulk viscosity with molecular rotors becomes possible. The principle of increasing quantum yield in solvents of higher viscosity is demonstrated in Fig. 6. Viscosity was modulated with mixtures of ethylene glycol and glycerol, which have different viscosities but somewhat similar polarity. Emission intensity follows a power–law relationship as predicted in (5). Linear regression yields exponents $x = 0.54$ in both cases and intercept values C_0 (the value of C for a viscosity of unity) of $C_0 = 144 \times 10^3$ for CCVJ and $C_0 = 71 \times 10^3$ for DCVJ.

Neither the rigorous derivation of the viscosity sensitivity by Förster and Hoffmann nor the more empirical derivation by Loutfy et al. account for all experimentally observed phenomena. More recently, molecular simulations have been employed to model the interaction between molecular rotors and the solvent. Parusel examined the energy states and dipole moments of DMABN derivatives to examine whether a planar or twisted configuration in the ground state accounts for the dual emission [34] and ruled out a mechanism where the molecule is twisted in the ground state and planar in the excited state (known as PICT mechanism), leaving the TICT mechanism as acceptable model. In addition, Parusel and Köhler found that the chain length of the donor group plays only a minimal role in the photophysical properties of DMABN derivatives [35]. Quiñones et al. [36] performed electronic structure modeling of DMABN in the gas phase and in the presence of polar solvents. In the gas phase, they found that DMABN assumes a nonplanar conformation where the dimethylamino group bends – rather than rotates – out of the molecule plane (“wagging angle”), whereas DMABN assumes a fully

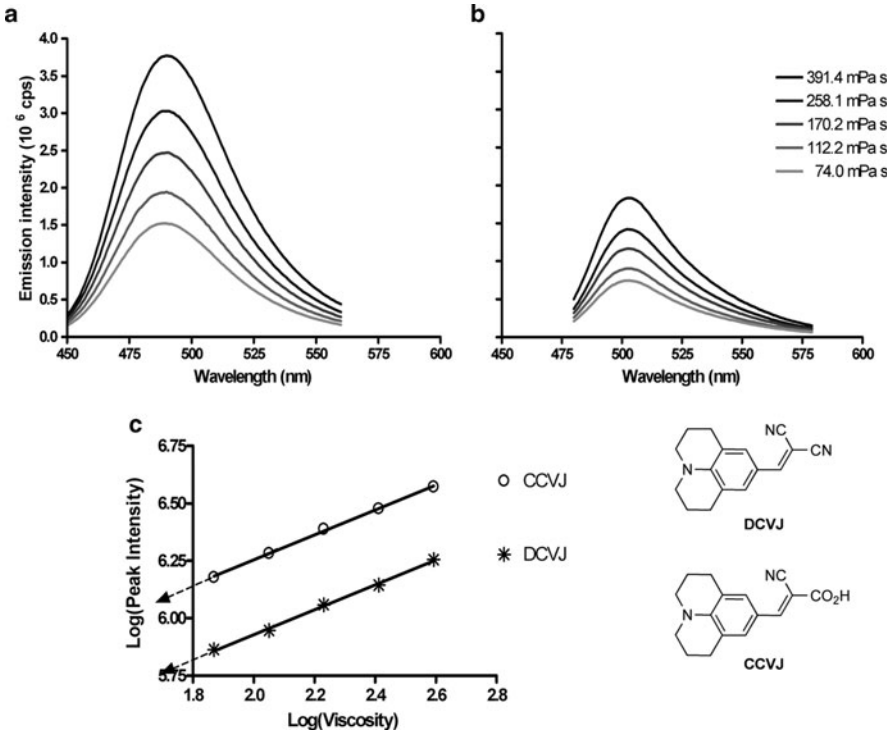

Fig. 6 Emission spectra of the molecular rotors CCVJ (**a**) and DCVJ (**b**) in a viscosity gradient with different mixture ratios of ethylene glycol and glycerol. As predicted by (5), a higher emission intensity, caused by a higher fluorescent quantum yield, is seen in higher-viscosity solvents. Plotting the peak intensities as a function of viscosity in a double-logarithmic scale reveals the power–law relationship described in (5), and the constants x and C can be determined from the diagram: x is the slope of the regression line, and C is the extrapolated intercept (*arrows*) of the regression lines with log(viscosity) $= 0$ or $\eta = 1$ m Pa s

planar conformation in the presence of polar solvents. In a related study, Zerner et al. [37] investigated ICT complexes with a malononitrile ($NC–CH_2–CN$) acceptor group, and compared the measured absorption spectra of an extensive number of structurally related compounds with computationally determined behavior, particularly in the presence of solvents. In a similar manner, Cao et al. [38] examined a hemicyanine dye that belongs to the popular group of stilbene-derived molecular rotors, and Allen et al. [14] studied the photophysical properties of DCVJ, one of the most widely applied molecular rotors. Structural changes and fluorescent response were simulated by Sudholt et al. [39] in a simulation of 255 molecules (one molecule being DMABN, surrounded by 254 solvent molecules). Structural changes, energy levels, spectral shifts, and lifetime dynamics were reported in vacuum and under influence of cyclopentane and acetonitrile as solvents. An overview of quantum chemical calculations performed with DMABN and related compounds can be found in a comprehensive review paper by Grabowski et al. [3]

together with an in-depth overview of the physical-chemistry foundations of molecular rotors. Whereas quantum chemical computations and molecular simulations have become more prominent in recent years, additional high-level models that reflect temperature, multiple solvents, and solvents in motion would further advance the understanding of TICT molecules with their environment. In addition, a shift of the focus from DMABN to the class of single-emission molecular rotors would reflect the latter's dominant use in practical applications.

3 Chemical Classes of Molecular Rotors

A large number of fluorophores builds on the ICT mechanism. It is therefore not surprising that the formation of TICT states has been observed in a large number of structurally different compounds. Common to the structure of all molecular rotors is a motif that consists of an electron donor unit in π-conjugation with an electron acceptor group. This motif is shown in Fig. 7. The universal donor group (electron donating group, EDG) is an alkylated nitrogen atom. The acceptor groups (electron accepting group, EAG) vary significantly and include functionalities such as nitriles, carboxylic esters, or aromatic rings. The two groups are connected via a π-conjugation system that facilitates electron transfer from donor to acceptor upon photoexcitation. DMABN (**1**) is a representative example of such design. Modifications that do not alter the extent of π-conjugation between the donor and acceptor groups will be summarized in the class of DMABN-related structures. Extension of the π-conjugation system increases the distance between the donor and acceptor units and thus significantly changes the fluorescent profile of such probes. An example is the structure of (*p*-(dialky1amino)-benzylidene)malononitrile, DBMN (**2**) [33]. DBMN is one example of fluorophore that exhibits nonradiative deactivation from the TICT state, which occurs when the S_1–S_0 energy gap in the twisted state becomes much smaller than in the planar state (cf. Fig. 3). Within the class of DBMN-related structures are included molecules with longer π-conjugation motifs such as stilbenes and 2-dicyanomethylene-3-cyano-2,5-dihydrofuran (DCDHF) flurophores. A third class of molecular rotors includes triphenylmethane-based fluorophores, and one representative example is crystal violet

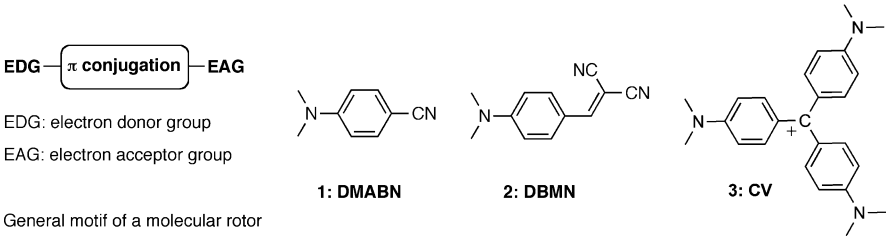

Fig. 7 General motif and representative structures of molecular rotors

[28]. In a separate class are included compounds such as porphyrins and BODIPY that have not yet been thoroughly explored as molecular rotors. A comprehensive review on porphyrin-based structures has been recently published [40]. The photophysical behavior of BODIPY dyes has been interpreted through the TICT mechanism [41, 42]. However, chemical computations by Kee et al. [41] present a very atypical picture where the planar excited-state configuration (0° or 180°) is energetically preferred with a lowest-energy angle of 55° in the ground state (only 35° from perpendicularity). A low degree of rotation would correspond to a low sensitivity toward the environment. Because the involvement of TICT states in the photophysical behavior of porphyrins and BODIPY has not conclusively been proven, these dyes are not covered in this chapter.

3.1 DMABN-Related Fluorescent Probes

3.1.1 Modifications of the Electron Donor Group

The general motif of DMABN (**1**) can be optimized for individual applications by modifying the electron donor or electron acceptor substituents. Often, such modifications have an effect on the sensitivity and overall fluorescent profile of the probes. The dimethyl amino donor of DMABN can be replaced by aliphatic or alicyclic amino groups. If there are no steric restrictions to the internal rotation, these probes exhibit the main characteristic features of DMABN with only some quantitative differences in sensitivity, radiative rates, and energy levels. Compounds **4** and **5** (Fig. 8) serve as an example of this approach: similar to DMABN, they both exhibit dual fluorescence, but the charge transfer band is more intense for **4** due to the larger ring structure of the donor group [43]. Related studies with dialkyl homologs of DMABN, such as **6** and **7**, have shown a preference for higher emission from the planar LE state as the length of the alkyl groups is increasing [12]. Based on this observation, it was proposed that increase of the alkyl group length increases the dipole moment of the molecule. This stabilizes the excited state and therefore leads to an increase of fluorescence intensity.

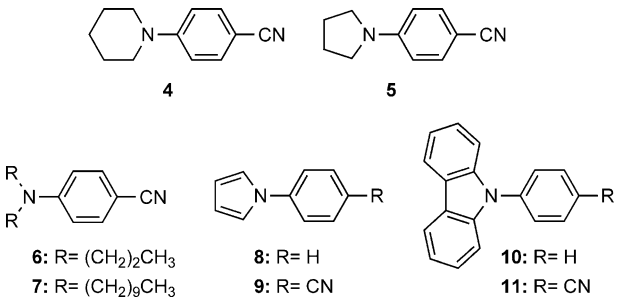

Fig. 8 Representative structures of DMABN-based rotors with different electron donor groups

Nitrogen-containing heteroaromatic rings have also been used as the electron donor groups (Fig. 8). In the case of pyrrole, the relatively low ionization potential of this ring produces a measurable fluorescence band from the LE state even when unsubstituted benzene is used as the acceptor (e.g., compound **8**). The absorption spectra of **8** and **9** show no significant changes in solvents of increasing polarity. However, the fluorescence emission of **9** is more red-shifted in polar solvents, presumably due to the electron accepting CN group. Carbazoles have a similar oxidation potential to pyrrole and can be also used as electron donors. Interestingly, **10** exhibits a solvent-independent fluorescence emission, whereas **11** behaves predictably as a molecular rotor.

3.1.2 Modifications of the π-Conjugation System

Substitution at the periphery of the phenyl ring plays a minor role in the fluorescent profile of the probe unless they affect the rotation of the donor group. For example, both compounds **12** and **13** (Fig. 9) have dual fluorescence that is similar to DMABN [44]. However, the steric congestion that is due to substitution at the periphery of the phenyl ring can destabilize the planar structure of the excited state and increase the rate of crossing to a twisted state. For instance, compound **13** has a more pronounced charge transfer band than compound **12**. Similarly, substitution of the phenyl ring with electron donating groups, such as in compound **14**, results in only small differences in the fluorescent profile of this probe as compared to DMABN [45]. In the cases of polysubstituted phenyl rings, the steric effects dominate over the electronic effects [46].

Replacing the phenyl group by a naphthalene reduces the energy gap between the LE and the charge transfer state. Compound **15** emits a dual fluorescence that was interpreted in terms of the TICT model [47]. The presence of the donor and acceptor groups along the long axis of naphthalene of rotor **16** increases significantly both Stokes shift and intensity over **15**. This can be explained by considering that substituents along the long axis of naphthalene decrease significantly the lowest singlet excited state [6]. This results in an increase of the energy "hump"

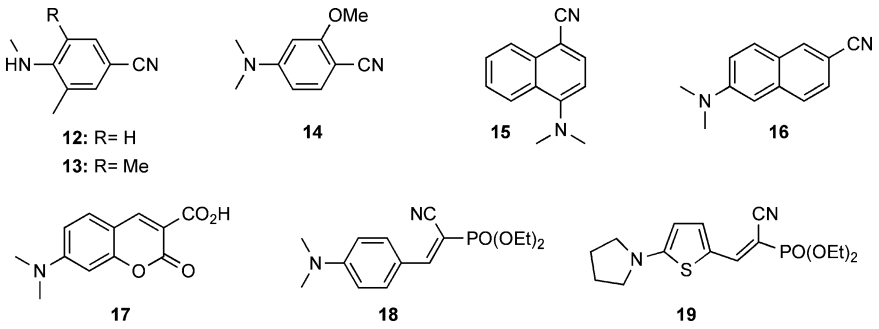

Fig. 9 Representative structures of DMABN-based rotors with different π-conjugation systems

between that excited state and the TICT state, thus rendering the compound brighter, but less sensitive to environmental changes. On the other hand, substituents along the short axis of naphthalene, such as in rotor **15**, decrease the second lowest excited state and thus increase the coupling of this state with the TICT states.

Replacing the phenyl group by a coumarin motif produces an important subclass of molecular rotors, represented by **17**, which have found several applications in viscosity and polarity measurements [48]. On the other hand, compound **19** has a red-shifted emission as compared to **18** due to the effective delocalization of the π-electrons in the presence of the thiophene chromophore [49].

3.1.3 Modifications of the Electron Acceptor Group

Replacing the nitrile by a carbonyl group does not significantly affect the fluorescence profile of the probe. For instance, dual fluorescence is observed for compounds **20** and **21** in polar solvents (Fig. 10). However, the fluorescence profile of the carboxylic acid-containing compound **20** is further complicated by the protolytic dissociation in the same solvents [50]. Moreover, esters with long carboxylic side chains, such as **22**, have been reported to form excimers in organic solvents [51]. In the case of amides, the substituents on the amide nitrogen can attenuate the acceptor effect. Thus, the nonsubstituted amide **23** is more red-shifted as compared to the fully substituted amide **24** [52]. Both amides have dual fluorescence in polar solvents, although with low quantum yields.

Replacing the nitrile group by a benzothiazole produces an important subclass of fluorescent compounds represented by thioflavin T (**25**, Fig. 10). It is not clear if this compound undergoes deactivation via intramolecular rotation that would meet the criterion for a molecular rotor. The steady-state absorption and emission properties of thioflavin T has been attributed to micelle formation [53, 54], dimer and excimer formation [55, 56], and deactivation through intramolecular rotation [57].

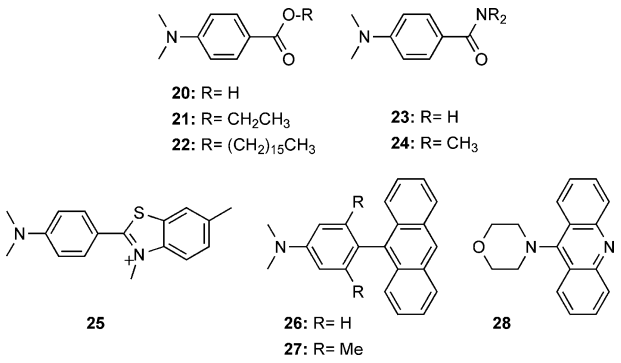

Fig. 10 Representative structures of DMABN-based rotors with different electron acceptor group

Anthracene has also been used as an acceptor (Fig. 10). In solution, **26** emits a single fluorescence band that is somewhat structured in nonpolar solvents and becomes broad and structureless with increasing polarity [58]. The strongly hindered molecule **27** also exhibits a similar behavior, but its absorption spectrum is better structured [59]. The rate of formation of a charge transfer state is higher for **27** than for **26**. Based on this observation, it appears that the twist around the anthryl–phenyl C–C bond plays a significant role in the fluorescence profile of the probes [60]. Acridines, such as **28**, behave similarly to anthracene except that acridine is a better electron acceptor [61].

3.2 DBMN-Related Structures

3.2.1 Julolidines

Incorporation of the nitrogen donor within a fused ring system, such as the tricyclic julolidine motif, prohibits rotation across the C–N bond. For this reason, compound **29** has a single fluorescence band that is not sensitive to the environment (Fig. 11). Compound **30** has an extended π-conjugation system, due to the additional double bond, which participates in the fluorescence excitation and emission of this molecule. This compound, widely known as DCVJ, exhibits a single-band fluorescence emission that is red-shifted compared to **29**. Photoexcitation of DCVJ takes place by electron transfer from the julolidine nitrogen to one of the nitrile groups. Relaxation takes place either via fluorescence emission or via nonradiative deexcitation from the TICT state that involves intramolecular rotation around the vinyl double bond. If such rotation is hindered by reduced molecular free volume (corresponding to high viscosity of the environment), the relaxation occurs via an increased fluorescence emission. In contrast, in solvents of low viscosity, the relaxation proceeds mainly via the nonradiative TICT pathway. Overall, this results in a fluorescence emission where the quantum yield depends on the viscosity of the environment in a power–law fashion as described in (5) [62].

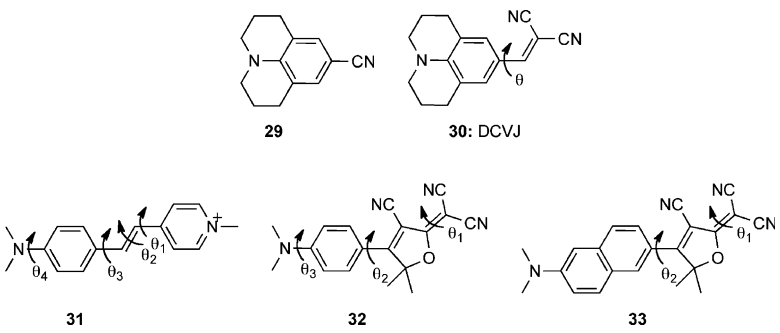

Fig. 11 Representative structures of DBMN-related structures with extended π-conjugation system

3.2.2 Stilbenes

Extending the conjugation between the donor and acceptor groups influences the fluorescence profile of the probes. A molecular rotor based on the stilbene motif is compound **31** (Fig. 11) [16]. One important difference to the aniline- and julolidine-based molecular rotors is the larger number of bonds around which the molecule can twist and form TICT states of different energy levels. Strehmel et al. [16] proposed that rotation around the three carbon–carbon bonds of the stilbene motif (θ_1, θ_2, and θ_3) is possible. In addition, rotation around the nitrogen–carbon bond of the dimethylamino donor is possible (θ_4), but it has a very low rotation rate due to a high energy barrier [16]. According to Strehmel et al. [16], rotation around the stilbene double bond is responsible for the creation of a lowered $S_1 - S_0$ energy gap that leads to radiationless relaxation from the twisted state, and this rotation mode is the preferred TICT mode, because there is no energy barrier between the planar and double-bond TICT state. Conversely, Cao et al. [38] and Pillai et al. [63] found that rotation around the stilbene double bond is not possible and attribute the radiationless relaxation from a TICT rotation around the bond marked with θ_3. Because of the larger number of bonds that allow twisted states, stilbene-based dyes show a more complex solvent interaction than aniline- or julolidine-based dyes. Similar observations have been reported for pyridinium- and diazene-based stilbenes [64].

3.2.3 2-dicyanomethylene-3-cyano-2,5-dihydrofuran (DCDHF) Fluorophores

The conjugation between the donor and acceptor groups can be extended by the incorporation of other ring structures, such as the dihydrofuran motif of compound **32** (Fig. 11) [65]. This has led to the design of the DCDHF fluorophores that exhibit two types of sensitivity to local environment: solvatochromism as a result of the charge transfer character of the excitation and viscosity dependence due to the suppression of the twisting motion that permits nonradiative deexcitation pathways. Extending the π-conjugation by replacing the phenyl ring with a naphthalene group (**33**) and other polyaromatic rings or modifying the substituents of the nitrogen donor can fine-tune the fluorescence profile of these molecules.

3.3 Ionic Dyes

The pioneering work Förster and Hoffmann [28] on the viscosity dependence of the fluorescence quantum yield of triphenylmethane dyes (TPM) has set the foundation for several reports in these dyes (Fig. 12). It was found that both an ability to twist around the carbocationic center and the donor–acceptor properties are important [66]. Specifically, a strong intramolecular quenching is observed for **34** that is virtually absent (two orders of magnitude slower quenching rate) in the bridged

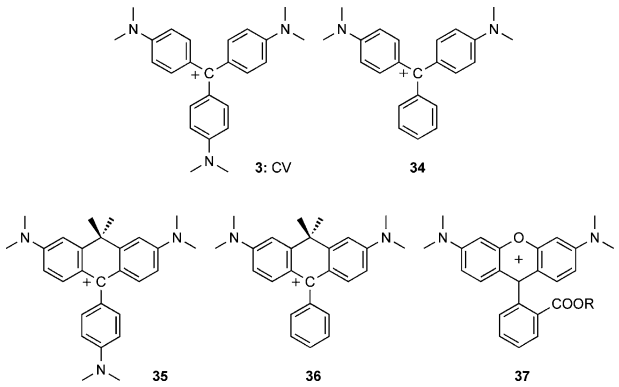

Fig. 12 Representative structures of triphenylmethane dyes

derivative **36**. Comparison of **3** with **35** shows that the quenching rate is only about ten times slower. This suggests that the flexibility of the third ring is not relevant to the fluorescence unless it contains a donor group. These observations also apply to related rhodamine dyes (compound **37**, Fig. 12) [67].

4 The Measurement of Molecular Rotor Fluorescence

Molecular rotors are useful as reporters of their microenvironment, because their fluorescence emission allows to probe TICT formation and solvent interaction. Measurements are possible through steady-state spectroscopy and time-resolved spectroscopy. Three primary effects were identified in Sect. 2, namely, the solvent-dependent reorientation rate, the solvent-dependent quantum yield (which directly links to the reorientation rate), and the solvatochromic shift. Most commonly, molecular rotors exhibit a change in quantum yield as a consequence of nonradiative relaxation. Therefore, the fluorophore's quantum yield needs to be determined as accurately as possible. In steady-state spectroscopy, emission intensity can be calibrated with quantum yield standards. Alternatively, relative changes in emission intensity can be used, because the ratio of two intensities is identical to the ratio of the corresponding quantum yields if the fluid optical properties remain constant. For molecular rotors with nonradiative relaxation, the calibrated measurement of the quantum yield allows to approximately compute the rotational relaxation rate k_{or} from the measured quantum yield ϕ_F through (9) [29],

$$\frac{k_{\mathrm{or}}}{k_r} = \frac{1}{\phi_F} - \frac{1}{\phi_0} \tag{9}$$

where k_r is the radiative relaxation rate and ϕ_0 is the quantum yield in the absence of rotational relaxation. The dye-dependent constants k_r and ϕ_F need to be determined

by other means. Often, ϕ_0 is set to unity for a rough approximation, and $k_r = \tau_0{}^{-1}$ is obtained from fluorescence in glass at 77 K. When the fluid is measured under conditions that alter the viscosity, but leave all other factors unchanged, the newly measured intensity F_2 relates to the altered viscosity η_2 through (5) and gives rise to (10),

$$\frac{F_2}{F_1} = \left(\frac{\eta_2}{\eta_1}\right)^x \tag{10}$$

because all dye-dependent constants in (5) as well as the instrument factors cancel out. Equation (10) can be solved for η_2 .This approach is feasible, for example, to measure temperature-induced changes or when measuring cells exposed to viscosity-modulating treatments [68].

Molecular rotors with a dual emission band, such as DMABN or *N*,*N*-dimethyl-[4-(2-pyrimidin-4-yl-vinyl)-phenyl]-amine (DMA-2,4; **38**, Fig. 13) [64], allow to use the ratio between LE and TICT emission to eliminate instrument- and experiment-dependent factors analogous to (10). One example is the measurement of pH with the TICT probe *p*-*N*,*N*-dimethylaminobenzoic acid **39** [69]. The use of such an intensity ratio requires calibration with solvent gradients, and influences of solvent polarity may cause solvatochromic shifts and adversely influence the calibration. Probes with dual emission bands often have points in their emission spectra that are independent from the solvent properties, analogous to isosbestic points in absorption spectra. Emission at these wavelengths can be used as an internal calibration reference.

A different approach to design a self-calibrating dye was proposed [70], in which a viscosity-sensitive molecular rotor (2-cyano-3-(4-dimethylaminophenyl) prop-2-enoic acid) was covalently linked to a reference dye, 7-methoxycoumarin-3-carboxylic acid, which exhibited no viscosity sensitivity (**40**, Fig. 13). A ratiometric measurement, that is, rotor emission relative to reference emission, was shown to be widely independent of dye concentration [70]. However, the design of such a ratiometric dye poses some challenges because of resonance energy transfer from

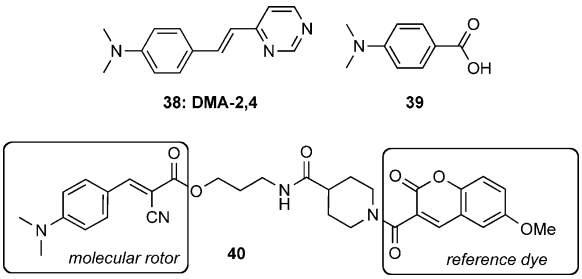

Fig. 13 Self-calibrating dyes DMA-2,4 and *p*-*N*,*N*-dimethylaminobenzoic acid. Compound **40** is an engineered ratiometric dye composed of a viscosity-sensitive molecular rotor and a nonviscosity-sensitive reference dye [70]

the shorter-wavelength dye to the longer-wavelength dye. With suitable filters, both emission bands can be acquired simultaneously. For this reason, such a dye is particularly attractive in microscopy experiments where local concentration changes would influence purely intensity-based results.

Another approach to reduce some of the influence of the instrument factors is by using specialized spectroscopic instruments with the capability to acquire additional information, namely, fluid absorption and scattering. Spectrofluorometers exist that can simultaneously acquire fluorescence emission and spectral absorption. In practice, it is difficult to distinguish dye absorption from fluid absorption, but dye concentration and its absorption coefficient are usually known. Therefore, a corrected emission intensity can be obtained that corresponds to the idealized emission intensity in the absence of solvent absorption. From the corrected intensity, the quantum yield can be deduced. Correction for fluid absorption becomes even more complex when the dye concentration is high and when the solvent absorption is strongly wavelength-dependent. The presence of scatterers further complicates the correction. In two relatively simple cases of forward-scattering microspheres and of starch solutions, the average excitation path length was found to be increased, and the presence of the scatterer increased fluorescence intensity. By measuring the scattering intensity, a corrected fluorescence emission was found that almost completely eliminated the influence of the scattering agent [71]. Higher scatterer content, however, would again reduce the measured intensity, and additional studies need to be performed to obtain correction formulas or algorithms for different types and concentrations of scatterers, and for combinations of scatterers and absorbers.

The measurement of fluorescent decay dynamics, i.e., fluorescence lifetime measurements, promise to overcome several of the challenges discussed above. Most importantly, lifetime and quantum yield are directly related through (11),

$$\phi_F = \frac{k_r}{k_r + k_{nr}} = \frac{\tau}{\tau_0} \tag{11}$$

where τ is the lifetime of the fluorophore and τ_0 is the natural lifetime, i.e., the lifetime in the absence of nonradiative processes (see (9)). Under consideration of (5), it can be seen that the lifetime τ is proportional to η^x, but without the instrument- and concentration-dependent factors that influence steady-state intensity. Calibration is still necessary to compute viscosity from lifetime, but fewer constants factor into the calibration for lifetime measurements than when steady-state intensity is used. However, molecular rotors typically exhibit extremely short lifetimes. Loutfy and Law [33] found lifetimes of *p-N,N*-dialkylaminobenzylidenemalononitriles between 3.2 and 11.1 ps in ethyl acetate. Ethyl acetate and many other solvents have a very low viscosity, and these lifetimes are typical for the types of molecular rotors with nonradiative relaxation from the TICT state. Many lifetime instruments are limited to the nanosecond to high picosecond range, and instruments that provide accurate results below 100 ps are usually specialized and expensive devices. However, specialized microscopes exist that allow spatially

resolved lifetime measurements, termed fluorescence lifetime imaging (FLIM). A FLIM microscope uses pulsed excitation and gated acquisition [72]. For this purpose, ultrafast lasers and a suitable high-speed, high-efficiency camera are required. Although this equipment is expensive and not readily available, the advantage of a straightforward calibration (11) and lifetime measurement widely independent of local variations of dye concentration makes this method attractive for cell studies.

Steady-state behavior and lifetime dynamics can be expected to be different because molecular rotors normally exhibit multiexponential decay dynamics, and the quantum yield that determines steady-state intensity reflects the average decay. Vogel and Rettig [73] found decay dynamics of triphenylamine molecular rotors that fitted a double-exponential model and explained the two different decay times by contributions from Stokes diffusion and free volume diffusion where the orientational relaxation rate k_{or} is determined by two Arrhenius-type terms:

$$k_{or} = A_{Stokes} \exp\left(-\frac{E_{Stokes}}{kT}\right) + A_{FV} \exp\left(-\frac{E_{FV}}{kT}\right) \tag{12}$$

Here, A_{Stokes} and A_{FV} are the contribution weights from Stokes- and free-volume diffusion, respectively, and E_{Stokes} and E_{FV} are the apparent activation energies for Stokes- and free-volume diffusion. Moreover, functional aspects of the solvent play an important role as well. It has been observed that polyfunctional alcohols, such as propanediol and glycerol, increase the orientational deactivation rate [73, 74], whereby single alcohols appear to have stick boundary conditions in the hydrodynamic model, and polyfunctional alcohols appear to have slip conditions, thus increasing diffusivity. Multiexponential relaxation dynamics that were dominated by solvent relaxation constants were also found by Dutta and Bhattacharyya [75], who reported lifetime constants in the low picosecond range, in the low nanosecond range, and higher, whereby the low nanosecond range carried significant information about the type of solvent, such as cyclodextrins, micelles, or polymers. Law [25] related relaxation times to the diffusional rotation of the solvent molecules, whereby rotational motion of the solvent molecules increased the rotational decay rate of the molecular rotors. Hara et al. [76] found triple-exponential decay functions when they applied pressure to the solvents to cause a pressure-induced viscosity increase. These few examples demonstrate to what extent lifetime experiments have the capability to reveal the complexity of the interaction of molecular rotors with their solvent. The analysis of lifetime experiments is complex, because many levels of solvent–rotor interaction, such as diffusion, electrostatic and polar interaction, and hydrogen bonding influence the lifetime dynamics and lead to complex decay patterns. This level of complexity cannot be seen in steady-state experiments, and it can be expected that lifetime experiments with instruments capable of capturing ultrashort decay rates provide a deeper insight into TICT dynamics and TICT-formation under the influence of different solvents.

5 Applications of Molecular Rotors

Much of this chapter covered the interaction of molecular rotors with the surrounding solvent. Elucidating this interaction is fundamental to the understanding of the TICT mechanism and, as the behavior of TICT fluorophores becomes better understood, leads to better understanding of the behavior of fluids. Of particular interest is the analysis of diffusion behavior, because it was found that molecular rotor fluorescence agrees more with a free-volume model [32, 77] than with the Debye–Stokes–Einstein model. The understanding of molecular rotors as free-volume probes leads to numerous practical applications where polymerization processes, covalent and electrostatic binding, and changes in microviscosity can be monitored in real-time. Examples where molecular rotors enjoy high popularity are polymer formation processes, sensing of conformational changes in proteins and other macromolecules, and physiological processes in the cell.

5.1 Measurement of Bulk Fluid Viscosity

Fluorescence-based bulk viscosity measurement is one application that advertises itself almost immediately, particularly with julolidine-derived molecular rotors where the quantum yield is widely independent from solvent polarity. Solving (5) for η and assuming proportionality of quantum yield and emission intensity leads to (13),

$$\eta = \xi \cdot F_{\mathrm{em}}^{1/x} \tag{13}$$

where F_{em} is the peak emission intensity, ξ combines instrument- and solvent-dependent factors with the constant C in (5), and x is the exponent introduced in (5). Bulk viscosity measurement with conventional rheometers is a tedious process that requires several minutes of measurement time, followed by meticulous cleaning of the equipment. Rheometers are generally sensitive and prone to errors. In contrast, fluorescent intensity measurements could be performed in seconds, and by using disposable cuvettes, no cleaning would be necessary. Experiments have shown that fluorescence-based fluid measurements have the potential to surpass mechanical measurements in precision [78]. Interestingly, molecular rotors react to bulk viscosity changes in the manner described by (13) even if the viscosity is modulated by macromolecules that are several orders of magnitude larger than the rotor molecule itself [78, 79]. Two challenges need to be overcome. First, the constants C, ξ, and x are dependent on the type of solvent (e.g., alcohols, protein solutions, colloid solutions) and need to be calibrated for each type of fluid. Moreover, hydrophobic protein binding of some molecular rotors needs to be considered, although hydrophilic derivatives can be found that minimize protein binding [80]. Second, absorption and turbidity of the fluid influence the intensity

measurement and need to be accounted for (see Sect. 4). Although the basic principle of bulk fluid viscosity measurement with molecular rotors has been established, more research is necessary before this method can supplement or replace conventional rheometry.

5.2 *Probing Polymerization Dynamics with Molecular Rotors*

The interdependence of free volume and quantum yield in TICT-forming fluorophores allows their use in probing static and dynamic changes of free volume for polymers and therefore as probes of polymerization dynamics [29]. In polymers, viscosity variations due to changes in temperature are often described with the Williams–Landel–Ferry (WLF) model [81]. Viscosity can be interpreted as a function of free volume (6) [32]. In (7), molecular rotors with nonradiative relaxation from the TICT state were introduced as free-volume probes. During polymerization, the mobility of molecular rotors is progressively hindered as more rigid polymeric structures are formed from monomers. Concurrently, the solvent viscosity increases and the free volume decreases, while the viscosity-dependent quantum yield of molecular rotors increases. In addition, the free volume V_f of polymer– diluent mixtures of glass-forming polymers changes with temperature according to (14) [82],

$$V_f = \frac{\alpha_p V_p T_{g,P} + \alpha_d (1 - V_p) T_{g,d}}{\alpha_p V_p + \alpha_d (1 - V_p)} \tag{14}$$

where V_p is the polymer volume fraction, $T_{g,P}$ is the polymer glass temperature, $T_{g,d}$ is the diluent glass temperature, α_p is the thermal expansion coefficient of the polymer, and α_d is the expansion coefficient of the diluent. Consequently, the reorientation rate of molecular rotors is influenced both by the chemical process and by temperature.

Mechanical and chemical methods for qualitative and quantitative measurement of polymer structure, properties, and their respective processes during interrelation with their environment on a microscopic scale exist. Bosch et al. [83] briefly discuss these techniques and point out that most conventional techniques are destructive because they require sampling, may lack accuracy, and are generally not suited for *in situ* testing. However, the process of polymerization, that is, the creation of a rigid structure from the initial viscous fluid, is associated with changes in the microenvironment on a molecular scale and can be observed with free-volume probes [83, 84].

Some TICT-forming fluorescent probes containing the *p-N,N*-dialkylamino benzylidene malononitrile motif (usually related to **30** in Fig. 11) have been applied to monitor and quantify polymerization reaction, crosslinking, chain relaxation,

thermal transitions and relaxations, degradations (thermal, photochemical, physical), transport of small molecules, microphase separation, crystallization, gelation, and gel swelling. It has been experimentally confirmed that absorption and fluorescence maximum of these dyes move to longer wavelengths with an increase of the environment's dielectric constant. For dye **30**, DCVJ, the quantum yield increased markedly as the medium underwent a transition from fluid to glass, a phenomenon attributed to a decrease in polymer free volume during polymerization [30]. In some specific examples, an increasing quantum yield accompanied by a decrease in nonradiative relaxation was observed during polymerization processes of water-soluble copolymers derived from 1-methyl-3-vinylpyridinium salts [85], methacrylate monomers [64], and polysaccharide polymers [48]. In another example, the polymerization process of polyacrylamide, type-I collagen and a tetramethoxysilane (TMOS) sol-gel was monitored with CCVJ (**41**, Fig. 14). Fluorescence steady-state intensity was related to the oscillatory behavior of magnetoelastic amorphous metal–glass. The emission intensity of CCVJ was increased in type-I collagen and TMOS sol-gel, but CCVJ was degraded by the ammonium persulfate in the polyacrylamide gel. On the other hand, CCVJ fluorescence provided distinctly different dynamics in the hydrolysis and crosslinking phases [86]. Benjelloun et al. [85] used a derivative of DMABN to monitor the formation of hydrophobic microdomains in amphiphilic polymers in water. The fluorescent probe exhibited enhanced emission from the LE band at higher concentrations of the polymers and with higher chain lengths, exposing the increased formation of hydrophobic microdomains. Zhu et al. [87] applied the hydrophobic molecular rotor FCVJ (CCVJ farnesyl ester **42**, Fig. 14) to obtain measurements of the relationship between viscosity and molecular weight (M) of polypropyleneoxide polymer melts. The hydrophobic nature of FCVJ allows it to integrate in a hydrocarbon-based polymer. For the polymer melts with low molecular weight (425–2,000 g mol^{-1}), viscosity followed the Rouse model that describes single-chain dynamics, and where viscosity is proportional to the molecular weight. Conversely, in polymer melts with high molecular weight (2.7–4 kg mol^{-1}), viscosity followed a power–law relationship with the molecular weight, $\eta \propto M^{3.4}$, which agrees with the reptation model, where a more complex chain interaction restricts the chain motion. Aggregation

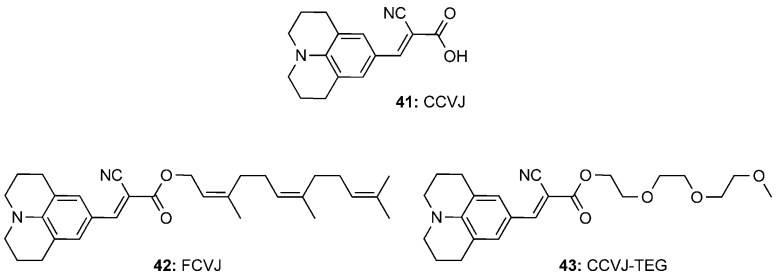

Fig. 14 Water-soluble CCVJ, hydrophobic CCVJ farnesyl ester (FCVJ) for cell membrane applications [88], and hydrophilic CCVJ triethyleneglycol ester (CCVJ-TEG) [89]

of proteins and saccharides are special cases of biopolymer formation and are discussed in detail in the next section.

5.3 *Applications of Molecular Rotors in Protein Sensing and Sensing of Other Macromolecules*

Most of the molecules introduced in this chapter are hydrophobic. Even those molecules that have been functionalized to improve water-solubility (for example, CCVJ and CCVJ triethyleneglycol ester **43**, Fig. 14) contain large hydrophobic structures. In aqueous solutions that contain proteins or other macromolecules with hydrophobic regions, molecular rotors are attracted to these pockets and bind to the proteins. Noncovalent attraction to hydrophobic pockets is associated with restricted intramolecular rotation and consequently increased quantum yield. In this respect, molecular rotors are superior protein probes, because they do not only indicate the presence of proteins (similar to antibody-conjugated fluorescent markers), but they also report a constricted environment and can therefore be used to probe protein structure and assembly.

Nile Red (**44**, Fig. 15), a highly polarity-sensitive fluorophore, is nearly quenched in aqueous solutions and emits at 570 nm in nonpolar solvents such as toluene, and peak emission ranges to 636 nm in polar liquids. Originally, this dye was used as a lipid and lipoprotein stain. Although some researchers describe Nile Red as a TICT molecule with electron transfer from the diethylamino group to the aromatic ring system, controversial explanations of its mechanism exist. According to the TICT interpretation, nonradiative relaxation form the TICT state dominates in polar solvents, but in nonpolar solvents, the TICT process is considered unfavorable and consequently the lifetime and quantum yield increase dramatically [90–92]. Other researchers suggest, in contrast to the TICT interpretation, that hydrogen bonding associated with solvent–dye interaction (i.e., alcohols) lowers the fluorescent lifetime via vibrational dissipation [93]. Whereas the actual mechanism is still under investigation, Nile Red sensitivity to environmental polarity is valuable in a variety of protein conformation investigations. For example, GRP94, the endoplasmic reticulum Hsp90 paralog (Heat shock protein 90) binds a variety of peptides. Using a known immunodominant peptide epitope of the vesicular stomatitis virus, acrylodan and Nile Red, the activation of peptide binding was found to be accompanied by enhanced peptide and solvent accessibility to hydrophobic binding sites [94]. This is just one of many examples of Nile Red's

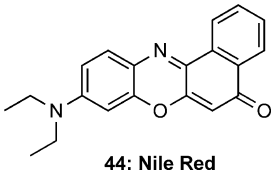

44: Nile Red

Fig. 15 Structure of Nile red

ability to determine aggregation, denaturation, and the conformation state of lipid/protein interfaces.

Thioflavin T (**25** in Fig. 10) was originally used to stain amyloid deposits in tissues [95] and later for the quantification of amyloid fibrils in the presence of precursor proteins [96, 97]. Thioflavin T interacts with the β-sheet structure of the amyloid protein along the shallow groove formed by adjacent Tyr and Leu residues on the surface [98, 99]. Applications with Thioflavin T have advanced from simple histological stains for connective tissue to more complex dual staining techniques that compensate for buffer conditions and species-specific backgrounds [100, 101]. Each experimental system should be carefully analyzed for possible misinterpretations. One example is 4,5-dianilinophthalimide (DAPH), which disintegrates amyloid fibers involved in Alzheimer's disease [102–104]. When DAPH was studied with β-lactoglobulin, a whey protein, Thioflavin T reported disintegration with decreased fluorescence, but birefringence and TEM tests did not. It was discovered that DAPH likely binds in the β sheet channels, thus hindering Thioflavin T binding [105] and disguising the low rate of β-lactoglobulin disintegration. Other applications of Thioflavin T include the direct observation of amyloid growth with total internal reflection microscopy [106] and ligand reactions at the acylation site of acetylcholinesterase [107]. Thioflavin T can also be used with other types of helical structures. It has been demonstrated that Thioflavin T can bind to Type I collagen prepared from the atelocollagen of yellowfin tuna skin [108]. Transthyretin, a thyroid hormone carrier, is a protein linked to amyloid diseases such as senile systemic amyloidosis and familial amyloidotic polyneuropathy and was investigated with several TICT dyes, 1-anilinonaphthalene-8-sulfonate (ANS), 4-4-*bis*-1-phenylamino-8-naphthalene sulfonate (*Bis*-ANS), 4-(dicyanovinyl)-julolidine (DCVJ), and Thioflavin T (ThT). Both steady-state and time-fluorescence assays, static and kinetic, characterized the protofibrillar states exposing conformational changes, aggregation, and misfolding [109].

Conformation and aggregation of proteins are not the only macromolecule applications for TICT fluorophores. For example, Bosch et al. [110, 111] have developed a saccharide sensing molecule containing a boron–nitrogen bond that displays fluorescence in both the LE state and the twisted internal charge transfer state. Without the presence of saccharides (in this case, either D-fructose, D-glucose, D-galactose, or D-mannose), the molecule emits at 404 nm from its TICT state when excited at 274 nm. With the addition of saccharides, the B–N bond is broken and a boronate species forms. The fluorescent emission blue-shifts to 362 nm (the LE state emission) since the nitrogen lone pair is free to conjugate with the π-system on the aniline component. Tan et al. [112] continued to modify this base structure to create another saccharide sensor, 4-*N*-methyl-*N*′-(2-dihydroxyborylbenzyl)-benzonitrile, a close derivative of the DMABN structure, and at the same time a boronate analog, which is a selective sensor for fluoride ions. Twisted intramolecular charge state fluorophores are also a valuable tool for nucleic acid–protein interactions. In Fig. 16, the fluorophore component **45** for nucleic acid monitoring is compared to DCVJ. The core fluorophore is conjugated to 5′-modified DNA and then mixed with bovine serum albumin (BSA) and single-stranded DNA binding protein

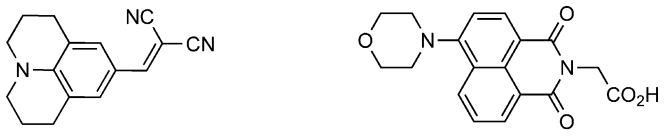

30: DCVJ **45**

Fig. 16 DCVJ compared to the core fluorophore for the DNA–Dye–BSA/SSP assay (**45**). The 5′ DNA strand is conjugated to the carboxylic acid group, leaving the morpholine group to access the hydrophobic pockets

(SSP). In the presence of BSA, the fluorescence intensity increased (expressed as a ratio against dye–DNA alone) indicating preference for the hydrophobic pocket where a potential TICT mechanism is associated with inhibited intramolecular rotation. When SSP was added, the fluorescent intensity decreased, indicating that the fluorophore was removed from the hydrophobic pockets [113]. As a probe, this assay could be tuned for a variety of protein–DNA monitoring in biological mixtures. Further study into the photophysical energy states during each phase of the assay could give interesting insight into complex biological processes.

A popular group of macromolecules are cyclodextrins, artificial polysaccharides that form a nanoscale truncated hollow cone with hydrophilic ends and a hydrophobic core. Cyclodextrins can be used to deliver hydrophobic substances to aqueous environments (e.g., drug delivery [114]), or they can withdraw hydrophobic or organometallic compounds from solutions. The exact nature of the hydrophobic core, particularly with respect to the formation of interlocked molecular systems (rotaxanes) and with respect to cyclodextrin dimer formation are still under investigation, and molecular rotors advertise themselves as probes for the restricted microenvironment of the cyclodextrin hydrophobic core. The principle of the interaction of cyclodextrins with a fluorophore can be demonstrated with the polarity-sensitive probe 6-propionyl-2-(dimethylamino)naphthalene (PRODAN). Although TICT formation of PRODAN is debated, the strong red-shift of the probe in polar media is well documented. In a study by Al-Hassan and Khanfer [115], PRODAN binding to cyclodextrin is demonstrated. Aqueous solutions of PRODAN and α-cyclodextrin, the smallest cyclodextrin with six glucopyranoside units, did not show a difference to aqueous PRODAN solution in the absence of cyclodextrin, but a blue-shift and increase of emission intensity was observed in solutions of β-cyclodextrin (seven glucopyranoside units) and γ-cyclodextrin (eight glucopyranoside units). The blue-shift indicates that the dye migrates into the hydrophobic cyclodextrin core. The migration process can be observed in time-resolved spectroscopy [115], where equilibration takes place with a time constant of several hours. Similar observations were made by Nakamura et al. with DMABN and glucosyl-conjugated β-cyclodextrin. Emission intensity of both DMABN emission bands increased upon association with cyclodextrin, and from the spectra, Nakamura et al. determined the association constants. Furthermore, a higher concentration of DMABN caused multiple DMABN molecules to be captured in the hydrophobic cavity, and their mutual influence increased the polar (red-shifted or

TICT) emission band. Similarly, the presence of other solvents increased the polar emission band, indicating that solvent molecules accumulated inside the cyclodextrin cavity and caused DMABN to react to the more polar environment. With a carboxylic-acid analog of DMABN, *p*-(*N*,*N*-diethylamino)benzoic acid (DEABA), Kim et al. [116] examined hydrogen-bonding effects in α- and β-cyclodextrins. Analysis of the fluorescent spectra and lifetimes allowed to conclude that DEABA associates differently with α- and β-cyclodextrins. The size of DEABA was estimated to be 9.3 Å long and 6.2 Å wide. Consequently, the diethylamino group would not fit into the core of α-cyclodextrin (diameter of 5 Å), forcing the carboxy group into the core. Conversely, β-cyclodextrin with an inner diameter of 6.5 Å allows the diethylamino group to fit; this is the preferred orientation due to the hydrophobic nature of the core. In this case, however, the carboxylic group is exposed to the solvent. In β-cyclodextrin, the red-shifted TICT emission increases, whereas in α-cyclodextrin, the TICT band decreases relative to the LE band. Similar results were reported by Panja and Chakravorti [117] who associated α-cyclodextrin with 4-*N*,*N*-dimethylamino cinnamaldehyde (DMACA) and found that two different configurations existed: first, where the dimethylamino group was inside the cavity and second, where the but-2-enal group was inside the cavity. Wang et al. [118] demonstrated that a DMABN-cyclodextrin combination can act as a biosensor. Wang et al. covalently bound DMABN and biotin to β-cyclodextrin and found that the presence of avidin and cholic acid analogs increased the LE emission of DMABN, indicating that the proximity of avidin and some cholic acid analogs exerted a nonpolar influence on the DMABN fluorophore.

5.4 Molecular Rotors as Microviscosity Probes in the Cell

Cellular biomechanics are primarily determined by the cell membrane, the cytoskeleton, and the cytoplasm. Whereas the cytoskeleton can be imagined as a relatively rigid framework, both the cytoplasm and the cell membrane have viscoelastic properties that change in various states of disease. The cell membrane plays a particularly important role since its viscosity influences the activity of membrane-bound proteins [119]. Consequently, changes in membrane viscosity have been linked with alterations in various physiological processes in the cell, particularly in conjunction with some disease states. Increased viscosity of red blood cell and platelet membranes has been observed in diabetic patients, and the viscosity change has been proposed to contribute to the reduced ability of the insulin receptor (a membrane-bound protein) to undergo aggregation [120, 121]. On the other hand, decreased membrane viscosity in leukocytes of patients with Alzheimer's disease has been postulated to facilitate aggregation of the Amyloid Precursor Protein (a transmembrane protein), a fragment of which is deposited in the brain as insoluble plaque [122]. Patients with liver disorders, including alcoholism-based diseases, showed higher erythrocyte membrane viscosity, which correlates highly with the severity of liver dysfunction [123]. Moreover, increased membrane

viscosity in leukocytes has been connected to the aging process [124]. These examples constitute only a few examples of an enormous literature body on the relationship between cell membrane viscosity and disease.

The effects of cytoplasmic viscosity are widely unexplored. This may be attributed to the relatively difficult measurement methods available. In the cytoplasm, magnetic microparticles were predominantly used to obtain information on viscoelastic properties [125–127]. Clearly, the use of magnetic microparticles demands the use of very expensive equipment; the observation of the particles is time-consuming, thus limiting temporal resolution, and the interaction between the particles and the cellular environment may also cause measurement artifacts.

It becomes clear that the investigations related to the viscosity of cellular components strongly depends on the availability of viscosity probing methods that allow detection of viscosity changes on a microscopic scale and with very short response times. Fluorescence-based methods advertise themselves, because they meet the two demands of high spatial and temporal resolution. Two widely used methods to obtain viscosity information, predominantly employed in the cell membrane, are fluorescence recovery after photobleaching (FRAP) and fluorescence anisotropy. Both methods are very different from each other, but both use the diffusivity of specific fluorophores to obtain information about the viscosity of the environment. More recently, molecular rotors have been employed as microviscosity probes in the cell. Each of the three fluorescent methods has its own advantages and disadvantages. FRAP has been established as the gold-standard of membrane viscosity measurement, but a single recovery experiment may take several minutes, and the bleached spot size must be chosen to balance high spatial resolution (small spot) with low noise and low measurement errors (large spot). The bleaching pulse introduces energies high enough to cause protein crosslinking and free radical formation, which may alter the environment, particularly in live cells. Moreover, the necessary confocal equipment is costly. Anisotropy experiments can be performed with conventional epifluorescent microscopes, and anisotropy measurements have a dramatically better spatial and temporal resolution than FRAP. On the other hand, local viscosity can only approximately be computed from the polarization anisotropy ratio, and any minor misalignment or imperfection of the polarizers – including any tendency of lasers or monochromators to polarize light – causes major measurement errors. By using molecular rotors, the simplest equipment is sufficient, and emission intensity from molecular rotors can be observed in real time and with a spatial resolution limited only by the optical system. On the other hand, intensity-based measurements can be confounded by local concentration changes, illumination inhomogeneities, and optical properties (scattering, absorption) of the sample. As introduced in Sect. 4, relative measurements, ratiometric dyes, and lifetime imaging can eliminate some of the confounding factors.

Early studies focused on the behavior of molecular rotors in vesicles [128] and lipid bilayers [18, 26]. Humphrey-Baker et al. [128] found that an indocyanine dye associates with micellar systems in aqueous suspension. The dye migrates into the micelles and shows an increased quantum yield and a bathochromic shift of emission. Although Humphrey-Baker et al. identify modulation of the quantum

yield by rigidization of the dye in the hydrophobic environment of the micelles, a detailed explanation of TICT formation is not given. Kung and Reed [18] performed spectroscopic studies of DCVJ in several solvents and liposome preparations. Kung and Reed found a weak linear relationship between the solvent's dielectric constant and peak emission wavelength where the full range from nonpolar (benzene) to polar (alcohols) caused less than 30 nm of bathochromic shift. A viscosity gradient created with mixtures of alcohols demonstrated the power–law relationship between viscosity and quantum yield (5) with exponent $x = 0.6$. In DPPC liposomes, a sharp change of the exponent was seen when the temperature was increased over the transition temperature. This experiment demonstrates how a molecular rotor reflects the sudden change in free-volume behavior in phospholipids between the gel and the liquid-crystal phase. This effect was later exploited by our own group to validate the viscosity-sensitivity of molecular rotors bound to the hydrophobic tails of phospholipids [129]. Lukac [26] found a very similar behavior when examining a derivative of (*p*-(dialkyl amino)-benzylidene)malononitrile in DPPC and DSPC vesicles. Interestingly, Lukac found a more pronounced temperature-dependent bathochromic shift in DSPC vesicles than in DPPC vesicles, which was attributed to a different localization of the molecular rotor in DSPC vesicles with their longer tail chains. The study by Kung and Reed demonstrated a key advantage of julolidine-based molecular rotors, namely, the separation of the effects of polarity and viscosity, which only influence peak emission and quantum yield, respectively [18]. This effect was later confirmed in similar studies [14, 19]. More recently, Nipper et al. [130] related apparent viscosity reported by FCVJ (**42**) and apparent viscosity reported by FRAP and found a linear relationship with good correlation.

Molecular rotors were also used in several studies to probe live cells, namely, the cell membrane, the cytoplasm, and the cytoskeleton. Viriot et al. [27] present a review of applications of several conjugated molecular rotors to probe microdomains in polymers, investigate the thermotropic behavior of liposomes, and stain the membranes of endothelial cells. Our own group has performed a number of studies related to changes in membrane viscosity in endothelial cells as a consequence of fluid shear stress. A study with DCVJ-stained cells showed a reversible decrease of membrane viscosity under fluid shear stress [68], allowing to conclude that the cell membrane is the most likely mechanoreceptor of the cell. DCVJ has a high affinity for hydrophobic parts of the cell, including the cell membrane and the cytoskeleton. We found that interior parts of endothelial cells were stained with DCVJ, which diminishes the relative fluorescent response from the membrane. For this reason, we sought DCVJ derivatives that were more membrane-specific. Two notable derivatives were FCVJ and CCVJ-conjugated phospholipids [129]. The phospholipid-bound molecular rotors were shown to be highly sensitive viscosity probes in liposomes and cultured endothelial cells [129], but they also showed a certain cytotoxicity, likely because the introduction of the phospholipids changes the natural phospholipid composition of the membrane. Hydrocarbon chains like geranyl and farnesyl are known to improve membrane localization [131, 132]. Consequently, membrane localization of the CCVJ farnesyl ester (FCVJ) was improved

over DCVJ, and intensity responses were dramatically stronger [88]. A particularly interesting application is the examination of lipid rafts with molecular rotors. Pure intensity-based microscopy, for example with DCVJ, will be confounded by locally elevated concentration in the caveolin-rich lipid rafts [133], but ratiometric dyes and lifetime methods may overcome this challenge.

Fewer studies have focused on the cell cytoplasm. One challenge is the geometric inhomogeneity of the cell cytoplasm, where thickness and local concentration gradients influence the measured intensity. Luby-Phelps et al. [134] proposed to use the indocyanine dyes Cy3 and Cy5 as a dye pair where Cy3 acts as a molecular rotor with viscosity-dependent nonradiative deactivation channel, and the relatively rigid Cy5 acts as reference fluorophore. Fluorescence excitation and emission differ by about 100 nm between those dyes. Luby-Phelps et al. performed microinjection of the dye mixture into cells followed by ratiometric microscopic imaging and found that cytoplasmic viscosity was not significantly higher than water and did not significantly vary over the projected cell area. Conversely, Kuimova et al. [135] performed lifetime imaging on cells stained with an indacene-derived dye. The lifetime τ of the dye depended on the viscosity η of its environment with $\tau = z\,\eta^{\alpha}$ where z and α are constants that were calibrated with alcohol mixtures. In lifetime imaging, the lifetime τ is spatially resolved. Kuimova et al. found viscosity values of 140 ± 40 mPa s in contrast to the values found by Luby-Phelps. However, the microscopy images in the study by Kuimova et al. [135] exhibited a grainy distribution of the dye, which may be an indication that the dye was either preferentially bound to proteins or underwent micelle formation. Whereas Cy3 and Cy5 are water-soluble by merit of a charged nitrogen atom, the indacene dye with its weak dipole between the N^{+}–B^{-} pair and its long aliphatic chain appears to be widely hydrophobic. Protein binding of the indacene dye could explain the discrepancy.

The cellular cytoskeleton, primarily composed of microfilaments, microtubules, and intermediate filaments, provides structural support and enables cell motility. The cytoskeleton is composed of biological polymers and is not static. Rather, it is capable of dynamic reassembly in less than a minute [136]. The cytoskeleton is built from three key components, the actin filaments, the intermediate filaments, and the microtubules. The filaments are primarily responsible for maintaining cell shape, whereas the microtubules can be seen as the load-bearing elements that prevent a cell from collapsing [136]. The cytoskeleton protects cellular structures and connects mechanotransductive pathways. Along with mechanical support, the cytoskeleton plays a critical role in many biological processes.

Two of the cytoskeletal components, the actin filaments and the microtubules have been studied with molecular rotors. The main component of the actin filaments is the actin protein, a 44 kD molecule found in two forms within the cell: the monomeric globulin form (G-actin) and the filament form (F-actin). Actin binds with ATP to form the microfilaments that are responsible for cell shape and motility. The rate of polymerization from the monomeric form plays a vital role in cell movement and signaling. Actin filaments form the cortical mesh that is the basis of the cytoskeleton. The cytoskeleton has an active relationship with the plasma membrane. Functional proteins found in both structures

give actin the ability to form regions in the cell with distinct physical features. Such compartmentalization is often referred to as cell polarity. The microtubule structure is a tubular assembly of heterodimeric tubulin proteins. Tubulin is composed of α- and β- subunits that weigh around 55 kD each. Microtubules have distinct regions promoting growth from only one end. Any attempt to monitor tubule formation must focus on the advancing side of the chain. Microtubules participate in exocytosis, intracellular transport, spindle formation, and organism motility [137].

Traditional fluorophore–antibody staining has been extensively used to locate local concentrations of microfilaments and microtubules, and to track their growth. These techniques are limited by their ability to only detect a single target. When used to monitor actin aggregation, traditional fluorescent methods are limited by their ability to only measure concentration. It is the ability to track both monomeric and polymeric substrates that makes molecular rotors a powerful tool for studying protein reaction kinetics and protein assembly. The molecular rotor DCVJ has been established as a probe for monitoring bulk polymerization kinetics [83] and as a probe for various biological processes [27, 138]. The molecular rotor DCQ (1-(2-Hydroxyethyl)-6-[(2,2-dicyano)vinyl]-2,3,4-trihydroquinoline) has exhibited sensitivity to the polymerization of G-Actin to F-Actin [138, 139]. DCQ readily binds to actin, a process that is accompanied by an increase of DCQ emission intensity [138]. When actin is exposed to metallic ions, such as Mg^{2+}, a transformation from G-actin to F-actin takes place. This transformation is accompanied by a further increase of DCQ emission, and DCQ can be seen as a reporter for the conformational changes that actin undergoes during assembly. The molecular rotor DCVJ has been shown to preferentially bind to tubulin [140]. Kung and Reed [140] used DCVJ to observe DCVJ binding to tubulin and tubulin aggregation. DCVJ binding to tubulin proteins is accompanied with an increase of emission intensity that indicates hydrophobic, noncovalent binding with an accompanying restriction of intramolecular rotation. Assembly of DCVJ-carrying tubulin to higher-order microstructures was found to induce a conformational change in the region of the DCVJ binding site so as to further restrict the rotational mobility of the dye, and tubulin assembly can be monitored by increased DCVJ emission intensity. Moreover, the increase of emission intensity differs between tubulin sheets and microtubules, an observation that indicates differences in the morphology of sheet and tubular aggregates at the molecular level. With the ability to measure dynamic changes in both actin and tubulin, cytoskeletal changes can be tracked in real time and correlated with cellular function.

A more specialized application of molecular rotors in the cell is the measurement of intracellular potentials. Conventional techniques for measurements of potential in cells, organelles, and neurons have used microelectrodes as the main instrument for detection of changes in the cell potential. These techniques are technically challenging and unsatisfactory in terms of spatial resolution and signal-to-noise ratio. A number of styryl-related dyes emerged [141] where voltage-sensitivity was attributed to TICT formation [142]. Key to understanding the sensitivity of styryl dyes, such as aminostilbazolium (Fig. 17) is to recognize that there are two ground

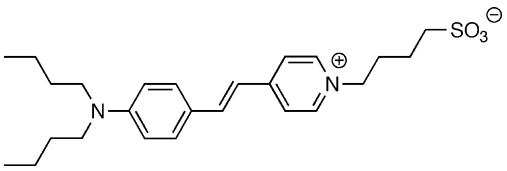

Fig. 17 Chemical structure of the styryl dye: (dibutylamino) stilbazolium butylsulfonate

states (the *cis*- and *trans*-isomers, separated by an energy barrier) and three relaxation modes, that is, regular fluorescence emission and nonradiative conversion into the *trans*-isomer, and a nonradiative deexcitation from a twisted state into either the *cis*-or the *trans*-isomer. Twisting takes place around the central double bond (θ_2 in Fig. 11). Isomerization of the aminostilbazolium dye from the *cis*- to the *trans*-state takes place predominantly in amphiphilic molecules and organic solvents. Ephard and Fromherz [142] suggest two possible mechanisms for the voltage sensitivity of aminostilbazolium in phospholipid membranes. First, an electrostatic field parallel to the molecule's main axis would interact with the excited-state redistribution of the charges in the molecule. Such a field would hinder a charge redistribution toward the anilino group, thus increasing the energy barrier that leads to the twisted state. Consequently, the horizontal transition rate into the twisted state is slowed down and fluorescence emission increases. Second, the electrostatic field could dislocate the dye inside the heterogeneous membrane/water interface, for example, by tilting the anilino group toward the aqueous phase. Consequently, the dye would experience a more polar environment with lower viscosity, and decreased fluorescence intensity would be observed. A later study by Jones and Bohn [143] showed that the presence of an electrostatic potential caused an increase in fluorescence intensity, which would indicate that the voltage-sensitivity of the dye is controlled by a charge redistribution that elevates the barrier for the TICT state, but Jones and Bohn interpret their experiments such that phospholipid protonation and dye dislocation are the predominant factors.

6 Future Directions

The examples in the previous section give a comprehensive overview of application areas where molecular rotors have become important fluorescent reporters. Current work on the further development of molecular rotors can broadly be divided into three areas: photophysical description, structural modification, and application development. Although a number of theories exist that describe the interaction between a TICT fluorophore and its environment, the detailed mechanism of interaction that includes effects such as polarity, hydrogen bonding, or size and geometry of a hydrophobic pocket are not fully understood. Molecular simulations have recently added considerable knowledge, particularly with

respect to the change of energy levels when the molecule undergoes conformational changes. However, few studies exist that provide detailed models of rotor–solvent interaction with multiple solvent molecules. Of particular interest are models that predict the interaction of molecular rotors with proteins, polymers that undergo polymerization, solvent mixtures, and solvent molecules with diffusional motion.

Chemical modifications of the structure are possible to optimize molecular rotors for specific applications. Examples are the functionalization of molecular rotors with recognition groups that allow specific protein binding, integration in a polymer matrix, or hydrophilic modifications that increase solubility and decrease the likelihood of binding to hydrophobic regions. Moreover, modifications of the actual molecular rotor dipole are possible to tune the photophysical properties [144]. All three elements of the EDG-π-EAG motif (Fig. 7) can be modified. It can readily be seen that an increased donor–acceptor distance causes a bathochromic shift and a tendency toward single emission from the LE state. Substitution of the π-system, for example, with a methoxy group, can increase the overall quantum yield. Additional points of rotation can be introduced (e.g., **38** in Fig. 13).

With further understanding how molecular rotors interact with their environment and with application-specific chemical modifications, a more widespread use of molecular rotors in biological and chemical studies can be expected. Ratiometric dyes and lifetime imaging will enable accurate viscosity measurements in cells where concentration gradients exist. The examination of polymerization dynamics benefits from the use of molecular rotors because of their real-time response rates. Presently, the reaction may force the reporters into specific areas of the polymer matrix, for example, into water pockets, but targeted molecular rotors that integrate with the matrix could prevent this behavior. With their relationship to free volume, the field of fluid dynamics can benefit from molecular rotors, because the applicability of viscosity models (DSE, Gierer–Wirtz, free volume, and WLF models) can be elucidated. Lastly, an important field of development is the surface-immobilization of molecular rotors, which promises new solid-state sensors for microviscosity [145].

7 Conclusion

A number of fluorescent dyes with internal charge transfer mechanism allow the molecule to twist (rotate) between the electron donor and electron acceptor moieties of the fluorescent dipole. In most cases, the twisted conformation is energetically preferred in the excited S_1 state, whereas the molecule prefers a planar or near-planar conformation in the ground state. For this reason, photoexcitation induces a twisting motion, whereas relaxation to the ground state returns the molecule to the planar conformation. Moreover, the $S_1 - S_0$ energy gap is generally smaller in the twisted conformation, and relaxation from the twisted state causes either a

red-shifted second emission band or – if the energy gap is small enough – nonradiative relaxation. These fluorescent molecular rotors are attractive as reporters in chemistry and biology, because the rate of twisted-state formation is influenced by the environment. Polarity plays a role in stabilizing the twisted state of some molecular rotors, and steric hindrance reduces TICT formation. The rate of TICT formation can therefore be determined with fluorescence steady-state or lifetime measurements. Very frequently, molecular rotors are employed as reporters for microviscosity, but the relationship between apparent viscosity and molecular-scale processes that influence TICT formation needs to be considered. Free-volume theory seems to be best suited to explain experimental results, predominantly the power–law relationship between bulk viscosity and quantum yield seen in some molecular rotors with nonradiative relaxation pathways. As such, molecular rotors have successfully been applied to probe polymerization and aggregation processes and to obtain spatially resolved local viscosity information. Whereas the molecular-level mechanisms of some TICT molecules, primarily aniline- and benzylidene malononitrile-related compounds are fairly well understood, the hypothesized involvement of twisted states in the fluorescent behavior of other families (e.g., porphyrins and BODIPY derivatives) is not fully understood and deserves more research.

References

1. Tomin V (2010) Physical principles behind spectroscopic response of organic fluorophores to intermolecular interactions. In: Demchenko AP (ed) Advanced Fluorescence Reporters in Chemistry and Biology I. Springer Ser Fluoresc 8:189–223
2. Rotkiewicz K, Grellmann KH, Grabowski ZR (1973) Reinterpretation of the anomalous fluorescence of p-N, N-dimethylaminobenzonitrile. Chem Phys Lett 19:315–318
3. Grabowski ZR, Rotkiewicz K, Rettig W (2003) Structural changes accompanying intramolecular electron transfer: focus on twisted intramolecular charge-transfer states and structures. Chem Rev 103(10):3899–4032
4. Rettig W, Lapouyade R (1994) Fluorescence probes based on twisted intramolecular charge transfer (TICT) states and other adiabatic photoreactions. Topics in fluorescence spectroscopy 4:109–149
5. Lapouyade R, Czeschka K, Majenz W, Rettig W, Gilabert E, Rulliere C (1992) Photophysics of donor–acceptor substituted stilbenes. A time-resolved fluorescence study using selectively bridged dimethylamino cyano model compounds. J Phys Chem 96(24):9643–9650
6. Zachariasse KA, Grobys M, von der Haar T, Hebecker A, Il'ichev YV, Jiang YB, Morawski O, Knhnle W (1996) Intramolecular charge transfer in the excited state. Kinetics and configurational changes. J Photochem Photobiol Chem 102(1S1):59–70
7. Grabowski ZG, Dobkowski J (1983) Twisted intramolecular charge transfer (TICT) excited states: energy and molecular structure. Pure Appl Chem 55(2):245–252
8. Gregoire G, Dimicoli I, Mons M, Donder-Lardeux C, Jouvet C, Martrenchard S, Solgadi D (1998) Femtosecond dynamics of "TICT" state formation in small clusters: the dimethylaminobenzomethyl ester acetonitrile system. J Phys Chem A 102(41):7896–7902
9. Rulliere C, Grabowski ZG, Dobkowski J (1987) Picosecond absorption spectra of carbonyl derivatives of dimethylaniline: the nature of the TICT excited states. Chem Phys Lett 137(5): 408–413

10. Bulgarevich DS, Kajimoto O, Hara K (1995) High-pressure studies of the viscosity effects on the formation of the twisted intramolecular charge-transfer (TICT) state in 4,4′-diaminodiphenyl sulfone (DAPS). J Phys Chem 99(36):13356–13361
11. Il'ichev YV, Kuhnle W, Zachariasse KA (1998) Intramolecular charge transfer in dual fluorescent 4-(dialkylamino) benzonitriles. Reaction efficiency enhancement by increasing the size of the amino and benzonitrile subunits by alkyl substituents. J Phys Chem A 102(28): 5670–5680
12. Schuddeboom W, Jonker SA, Warman JM, Leinhos U, Kühnle W, Zachariasse KA (1992) Excited-state dipole moments of dual fluorescent 4-(dialkylamino) benzonitriles. Influence of alkyl chain length and effective solvent polarity. J Phys Chem 96:10809–10819
13. Stsiapura VI, Maskevich AA, Kuzmitsky VA, Turoverov KK, Kuznetsova IM (2007) Computational study of thioflavin T torsional relaxation in the excited state. J Phys Chem A 111(22):4829–4835
14. Allen BD, Benniston AC, Harriman A, Rostron SA, Yu C (2005) The photophysical properties of a julolidene-based molecular rotor. Phys Chem Chem Phys 7(16):3035–3040
15. Rettig W, Strehmel B, Majenz W (1993) The excited states of stilbene and stilbenoid donor–acceptor dye systems. A theoretical study. Chem Phys 173(3):525–537
16. Strehmel B, Seifert H, Rettig W (1997) Photophysical properties of fluorescence probes. 2. A model of multiple fluorescence for stilbazolium dyes studied by global analysis and quantum chemical calculations. J Phys Chem B 101(12):2232–2243
17. Rettig W, Klock A (1985) Intramolecular fluorescence quenching in aminocoumarines. Identification of an excited state with full charge separation. Can J Chem 63(7):1649–1653
18. Kung CE, Reed JK (1986) Microviscosity measurements of phospholipid bilayers using fluorescent dyes that undergo torsional relaxation. Biochemistry 25:6114–6121
19. Haidekker MA, Brady TP, Lichlyter D, Theodorakis EA (2005) Effects of solvent polarity and solvent viscosity on the fluorescent properties of molecular rotors and related probes. Bioorg Chem 33(6):415–425
20. Diverdi LA, Topp MR (1984) Subnanosecond time-resolved fluorescence of acridine in solution. J Phys Chem 88(16):3447–3451
21. Guilbault GG (1990) Practical fluorescence. CRC, Boca Raton, FL
22. El-Sayed MA, Kasha M (1959) Interchange of orbital excitation types of the lowest electronic states of 2 ring N-heterocyclics by solvation. Spectrochim Acta 15:758–759
23. Haidekker MA, Akers W, Lichlyter D, Brady TP, Theodorakis EA (2005) Sensing of flow and shear stress using fluorescent molecular rotors. Sensor Lett 3:42–48
24. Kuimova MK, Botchway SW, Parker AW, Balaz M, Collins HA, Anderson HL, Suhling K, Ogilby PR (2009) Imaging intracellular viscosity of a single cell during photoinduced cell death. Nat Chem 1(1):69–73
25. Law KY (1980) Fluorescence probe for microenvironments: Anomalous viscosity dependence of the fluorescence quantum yield of p-N, N-dialkylaminobenzylidenmalononitrile in 1-alkanols. Chem Phys Lett 75(3):545–549
26. Lukac S (1984) Thermally induced variations in polarity and microviscosity of phospholipid and surfactant vesicles monitored with a probe forming an intramolecular charge-transfer complex. J Am Chem Soc 106:4386–4392
27. Viriot ML, Carré MC, Geoffroy-Chapotot C, Brembilla A, Muller S, Stoltz J-F (1998) Molecular rotors as fluorescent probes for biological studies. Clin Hemorheol Microcirc 19:151–160
28. Förster Th, Hoffmann G (1971) Die Viskositätsabhängigkeit der Fluoreszenzquantenausbeuten einiger Farbstoffsysteme [effect of viscosity on the fluorescence quantum yield of some dye systems]. Z Phys Chem 75:6376
29. Loutfy RO, Arnold BA (1982) Effect of viscosity and temperature on torsional relaxation of molecular rotors. J Phys Chem 86:4205–4211
30. Loutfy RO (1986) Fluorescence probes for polymer free-volume. Pure Appl Chem 58 (9):1239–1248

31. von Gierer A, Wirtz K (1953) Molekulare Theorie der Mikroreibung [Molecular theory of microfriction]. Z Naturforschung 8a:523–538
32. Doolittle AK (1952) Studies in Newtonian flow III. The dependence of the viscosity of liquids on molecule weight and free space (in homologous series). J Appl Phys 23(2): 236–239
33. Loutfy RO, Law KY (1980) Electrochemistry and spectroscopy of intramolecular charge-transfer complexes. p-N, N-dialkylaminobenzylidenemanononitriles. J Phys Chem 84: 2803–2808
34. Parusel ABJ (2001) Excited state intramolecular charge transfer in N, N-heterocyclic-4-aminobenzonitriles: a DFT study. Chem Phys Lett 340(5–6):531–537
35. Parusel ABJ, Köhler G (2001) Influence of the alkyl chain length on the excited-state properties of 4-dialkyl-benzonitriles. A theoretical DFT/MRCI study. Int J Quantum Chem 84(2):149–156
36. Quiñones E, Ishikawa Y, Leszczynski J (2000) Conformational properties of dimethylaminobenzonitrile in gas phase and polar solvents: ab initio HF/6-31G (d, p) and MP2/6-31G (d, p) investigations. J Mol Struct: THEOCHEM 529(1–3):127–134
37. Zerner MC, Reidlinger C, Fabian WMF, Junek H (2001) Push–dyes containing malononitrile dimer as acceptor: synthesis, spectroscopy and quantum chemical calculations. J Mol Struct: THEOCHEM 543(1–3):129–146
38. Cao X, Tolbert RW, McHale JL, Edwards WD (1998) Theoretical study of solvent effects on the intramolecular charge transfer of a hemicyanine dye. J Phys Chem A 102(17):2739–2748
39. Sudholt W, Staib A, Sobolewski AL, Domcke W (2000) Molecular-dynamics simulations of solvent effects in the intramolecular charge transfer of 4-(N, N-dimethylamino) benzonitrile. Phys Chem Chem Phys 2(19):4341–4353
40. Kottas GS, Clarke LI, Horinek D, Michl J (2005) Artificial molecular rotors. Chem Rev 105 (4):1281–1376
41. Kee HL, Kirmaier C, Yu L, Thamyongkit P, Youngblood WJ, Calder ME, Ramos L, Noll BC, Bocian DF, Scheidt WR (2005) Structural control of the photodynamics of boron–dipyrrin complexes. J Phys Chem B 109(43):20433
42. Kollmannsberger M, Rurack K, Resch-Genger U, Daub J (1998) Ultrafast charge transfer in amino-substituted boron dipyrromethene dyes and its inhibition by cation complexation: a new design concept for highly sensitive fluorescent probes. J Phys Chem A 102:10211–10220
43. Rettig W (1980) External and internal parameters affecting the dual fluorescence of p-cyano-dialkylanilines. J Lumin 26:21–46
44. Zachariasse KA, von der Haar T, Hebecker A, Leinhos U, Kuhnle W (1993) Intramolecular charge transfer in aminobenzonitriles: requirements for dual fluorescence. Pure Appl Chem 65(8):1745–1750
45. Rotkiewicz K, Rettig W, Detzerd N, Rothe A (2003) Substituent-induced coupling of the two lowest excited singlet states of 2-methoxy-derivatives of 4-(N, N-dimethylamino)- and 4-(N-methylamino)benzonitrile. Phys Chem Chem Phys 5:998–1002
46. Shinohara Y, Arai T (2008) Effect of methoxy substituents on the excited state properties of stilbene. Bull Chem Soc Jpn 81(11):1500–1504
47. Lippert E, Ayuk AA, Rettig W, Wermuth G (1981) Adiabatic photoreactions in dilute solutions of p-substituted N, N′-dialkylanilines and related donor–acceptor compounds. J Photochem 17:237–241
48. Even P, Chaubet F, Letourneur D, Viriot ML, Carre MC (2003) Coumarin-like fluorescent molecular rotors for bioactive polymers probing. Biorheology 40(1):261–263
49. Yang X, Jiang X, Zhao C, Chen R, Qin P, Sun L (2006) Donor–acceptor molecules containing thiophene chromophore: synthesis, spectroscopic study and electrogenerated chemiluminescence. Tetrahedron Lett 47:4961–4964
50. Cowley DJ, Peoples AH (1977) Rotational isomerism and dual luminescence in dipolar dialkylamino-compounds. J Chem Soc Chem Commun:352–353

51. Zhen Z, Tug C-H (1991) Hydrophobic effects on photophysical and photochemical processes: excimer fluorescence and aggregate formation of long-chain alkyl 4-(N, N-dimethylamino) benzoate in water–organic binary mixtures. Chem Phys Lett 180(3):211–215
52. Braun D, Rettig W, Delmond S, Letard J-F, Lapouyade R (1997) Amide derivatives of DMABN: a new class of dual fluorescent compounds. J Phys Chem A 101:6836–6841
53. Kumar S, Singh AK, Krishnamoorthy G, Swaminathan R (2008) Thioflavin T displays enhanced fluorescence selectively inside anionic micelles and mammalian cells. J Fluoresc 18(6):1199–1205
54. Khurana R, Coleman C, Ionescu-Zanetti C, Carter SA, Krishna V, Grover RK, Roy R, Singh S (2005) Mechanism of thioflavin T binding to amyloid fibrils. J Struct Biol 151(3): 229–238
55. Naik LR, Naik AB, Pal H (2009) Steady-state and time-resolved emission studies of thioflavin-T. J Photochem Photobiol A Chem 204:161–167
56. Retna Raj C, Ramaraj R (1997) Cyclodextrin induced intermolecular excimer formation of thioflavin T. Chem Phys Lett 273(3–4):285–290
57. Stsiapura VI, Maskevich AA, Kuzmitsky VA, Uversky VN, Kuznetsova IM, Turoverov KK (2008) Thioflavin T as a molecular rotor: fluorescent properties of thioflavin T in solvents with different viscosity. J Phys Chem B 112(49):15893–15902
58. Herbich J, Kapturkiewicz A (1991) Radiative and radiationless depopulation of the excited intramolecular charge transfer states: aryl derivatives of aromatic amines. Chem Phys 158:143–153
59. Siemiarczuk A, Grabowski ZR, Krówczynski A, Asher M, Ottolenghi M (1977) Two emitting states of excited p-(9-Anthryl)-N, N-dimethylaniline derivatives in polar solvents. Chem Phys Lett 51:315–320
60. Siemiarczuk A, Ware WR (1987) Complex excited-state relaxation in p-(9-Anthryl)-N, N-dimethylaniline derivatives evidenced by fluorescence lifetime distributions. J Phys Chem 91:3677–3682
61. Herbich J, Dobkowski J, Rulliére C, Nowacki J (1989) Low-temperature dual fluorescence in 9-morpholinoacridine picosecond TICT state formation? J Lumin 44:87–95
62. Haidekker MA, Theodorakis EA (2007) Molecular rotors-fluorescent biosensors for viscosity and flow. Org Biomol Chem 5(11):1669–1678
63. Pillai ZS, Sudeep PK, George Thomas K (2003) Effect of viscosity on the singlet-excited state dynamics of some hemicyanine dyes. Res Chem Intermed 29(3):293–305
64. Bosch P, Peinado C, Martin V, Catalina F, Corrales T (2006) Fluorescence monitoring of photoinitiated polymerization reactions synthesis, photochemical study and behaviour as fluorescent probes of new derivatives of 4-dimethylaminostyryldiazines. J Photochem Photobiol A Chem 180(1–2):118–129
65. Lord SJ, Conley NR, Lee HD, Nishimura SY, Pomerantz AK, Willets KA, Lu Z, Wang H, Liu N, Samuel R, Weber R, Semyonov A, He M, Twieg RJ, Moerner WE (2009) DCDHF fluorophores for single-molecule imaging in cells. ChemPhysChem 10:55–65
66. Rettig W, Vogel M, Lippert E, Otto H (1986) The dynamics of adiabatic photoreactions as studied by means of the time structure of synchrotron radiation. Chem Phys 103:381–390
67. Vogel M, Rettig W (1985) Efficient intramolecular fluorescence quenching in triphenylmethane dyes involving excited states with charge separation and twisted conformations. Ber Bunsenges 89(9):962–968
68. Haidekker MA, L'Heureux N, Frangos JA (2000) Fluid shear stress increases membrane fluidity in endothelial cells: a study with DCVJ fluorescence. Am J Physiol Heart Circ Physiol 278(4):H1401–H1406
69. Jiang Y (1994) pH Dependence of the twisted intramolecular charge transfer(TICT) of p-N, N-dimethylaminobenzoic acid in aqueous solution. J Photochem Photobiol A Chem 78 (3):205–208
70. Haidekker MA, Brady TP, Lichlyter D, Theodorakis EA (2006) A ratiometric fluorescent viscosity sensor. J Am Chem Soc 128:398–399

71. Milich KN, Akers W, Haidekker MA (2005) A ratiometric fluorophotometer for fluorescence-based viscosity measurement with molecular rotors. Sensor Lett 3:237–243
72. Suhling K, French PMW, Phillips D (2005) Time-resolved fluorescence microscopy. Photochem Photobiol Sci 4(1):13–22
73. Vogel M, Rettig W (1987) Excited state dynamics of triphenylmethane-dyes used for investigation of microviscosity effects. Ber Bunsenges Phys Chem 91:1241–1247
74. Moog RS, Ediger MD, Boxer SG, Fayer MD (1982) Viscosity dependence of the rotational reorientation of rhodamine B in mono- and polyalcohols. Picosecond transient grating experiments. J Phys Chem 86:4694–4700
75. Dutta P, Bhattacharyya K (2004) Ultrafast chemistry in complex and confined systems. J Chem Sci 116:5–16
76. Hara K, Bulgarevich DS, Kajimoto O (1996) Pressure tuning of solvent viscosity for the formation of twisted intramolecular charge-transfer state in 4, 4′-diaminophenyl sulfone in alcohol solution. J Chem Phys 104(23):9431–9436
77. Gierer VA, Wirtz K (1953) Molekulare Theorie der Mikroreibung. Z Naturforsch 8(Part A):532–538
78. Akers W, Haidekker MA (2005) Precision assessment of biofluid viscosity measurements using molecular rotors. J Biomech Eng 127(3):450–454
79. Akers W, Haidekker MA (2004) A molecular rotor as viscosity sensor in aqueous colloid solutions. J Biomech Eng 126(3):340–345
80. Akers WJ, Cupps JM, Haidekker MA (2005) Interaction of fluorescent molecular rotors with blood plasma proteins. Biorheology 42(5):335–344
81. Williams ML, Landel RF, Ferry JD (1955) The temperature dependence of relaxation mechanisms in amorphous polymers and other glass-forming liquids. J Am Chem Soc 84:2803–2808
82. Kelley FN, Bueche F (1961) Viscosity and glass temperature relations for polymer-diluent systems. J Polym Sci 50(154):549–556
83. Bosch P, Catalina F, Corrales T, Peinado C (2005) Fluorescent probes for sensing processes in polymers. Chem Eur J 11(15):4314
84. Paczkowski J, Neckers DC (1991) Twisted intramolecular charge-transfer phenomenon as a quantitative probe of polymerization kinetics. Macromolecules 24(10):3013–3016
85. Benjelloun A, Brembilla A, Lochon P, Adibnejad M, Viriot ML, Carré MC (1996) Detection of hydrophobic microdomains in aqueous solutions of amphiphilic polymers using fluorescent molecular rotors. Polymer (Guildford) 37(5):879–883
86. Haidekker MA, Lichlyter D, Ben Johny M, Grimes CA (2006) Probing polymerization dynamics with fluorescent molecular rotors and magnetoelastic sensors. Sensor Lett 4:257–261
87. Zhu D, Haidekker MA, Lee J-S, Won Y-Y, Lee JC (2007) Application of molecular rotors to the determination of the molecular weight dependence of viscosity in polymer melts. Macromolecules 40:7730–7732
88. Haidekker MA, Ling T, Anglo M, Stevens HY, Frangos JA, Theodorakis EA (2001) New fluorescent probes for the measurement of cell membrane viscosity. Chem Biol 8(2): 123–131
89. Haidekker MA, Brady TP, Chalian SH, Akers W, Lichlyter D, Theodorakis EA (2004) Hydrophilic molecular rotor derivatives-synthesis and characterization. Bioorg Chem 32(4): 274–289
90. Sarkar N, Das K, Nath DN, Bhattacharyya K (1994) Twisted charge transfer processes of Nile red in homogeneous solutions and in faujasite zeolite. Langmuir 10(1):326–329
91. Hazra P, Chakrabarty D, Chakraborty A, Sarkar N (2004) Intramolecular charge transfer and solvation dynamics of Nile red in the nanocavity of cyclodextrins. Chem Phys Lett 388(1–3): 150–157
92. Jee AY, Park S, Kwon H, Lee M (2009) Excited state dynamics of Nile red in polymers. Chem Phys Lett 477(1–3):112–115

93. Cser A, Nagy K, Biczók L (2002) Fluorescence lifetime of Nile red as a probe for the hydrogen bonding strength with its microenvironment. Chem Phys Lett 360(5–6):473–478
94. Wearsch PA, Voglino L, Nicchitta CV (1998) Structural transitions accompanying the activation of peptide binding to the endoplasmic reticulum Hsp90 chaperone GRP94. Biochemistry 37(16):5709–5719
95. Vassar PS, Culling CF (1959) Fluorescent stains, with special reference to amyloid and connective tissues. Arch Pathol 68:487
96. Voropai ES, Samtsov MP, Kaplevskii KN, Maskevich AA, Stepuro VI, Povarova OI, Kuznetsova IM, Turoverov KK, Fink AL, Uverskii VN (2003) Spectral properties of thioflavin T and its complexes with amyloid fibrils. J Appl Spectrosc 70(6):868–874
97. Wood SJ, Maleeff B, Hart T, Wetzel R (1996) Physical, morphological and functional differences between pH 5.8 and 7.4 aggregates of the Alzheimer's amyloid peptide A. J Mol Biol 256(5):870–877
98. Biancalana M, Makabe K, Koide A, Koide S (2009) Molecular mechanism of thioflavin-T binding to the surface of b-rich peptide self-assemblies. J Mol Biol 385(4):1052–1063
99. Wu C, Biancalana M, Koide S, Shea JE (2009) Binding modes of thioflavin-T to the single-layer beta-sheet of the peptide self-assembly mimics. J Mol Biol 394(4):627–633
100. Sen P, Fatima S, Ahmad B, Khan RH (2009) Interactions of thioflavin T with serum albumins: spectroscopic analyses. Spectrochim Acta Part A: Mol Biomol Spectrosc 74(1): 94–99
101. Eisert R, Felau L, Brown LR (2006) Methods for enhancing the accuracy and reproducibility of Congo red and thioflavin T assays. Anal Biochem 353(1):144–146
102. Blanchard BJ, Chen A, Rozeboom LM, Stafford KA, Weigele P, Ingram VM (2004) Efficient reversal of Alzheimer's disease fibril formation and elimination of neurotoxicity by a small molecule. Proc Natl Acad Sci U S A 101(40):14326
103. Feng BY, Toyama BH, Wille H, Colby DW, Collins SR, May BCH, Prusiner SB, Weissman J, Shoichet BK (2008) Small-molecule aggregates inhibit amyloid polymerization. Nat Chem Biol 4(3):197
104. Wang H, Duennwald ML, Roberts BE, Rozeboom LM, Zhang YL, Steele AD, Krishnan R, Su LJ, Griffin D, Mukhopadhyay S (2008) Direct and selective elimination of specific prions and amyloids by 4, 5-dianilinophthalimide and analogs. Proc Natl Acad Sci 105 (20):7159
105. Kroes-Nijboer A, Lubbersen YS, Venema P, van der Linden E (2009) Thioflavin T fluorescence assay for [beta]-lactoglobulin fibrils hindered by DAPH. J Struct Biol 165(3):140
106. Ban T, Hamada D, Hasegawa K, Naiki H, Goto Y (2003) Direct observation of amyloid fibril growth monitored by thioflavin T fluorescence. J Biol Chem 278(19):16462–16465
107. De Ferrari GV, Mallender WD, Inestrosa NC, Rosenberry TL (2001) Thioflavin T is a fluorescent probe of the acetylcholinesterase peripheral site that reveals conformational interactions between the peripheral and acylation sites. J Biol Chem 276(26):23282
108. Morimoto K, Kawabata K, Kunii S, Hamano K, Saito T, Tonomura B (2009) Characterization of type I collagen fibril formation using thioflavin T fluorescent dye. J Biochem 145(5): 677
109. Lindgren M, Sörgjerd K, Hammarström P (2005) Detection and characterization of aggregates, prefibrillar amyloidogenic oligomers, and protofibrils using fluorescence spectroscopy. Biophys J 88(6):4200–4212
110. Bosch LI, Mahon MF, James TD (2004) The B–N bond controls the balance between locally excited (LE) and twisted internal charge transfer (TICT) states observed for aniline based fluorescent saccharide sensors. Tetrahedron Lett 45(13):2859–2862
111. Arimori S, Bosch LI, Ward CJ, James TD (2001) Fluorescent internal charge transfer (ICT) saccharide sensor. Tetrahedron Lett 42(27):4553–4555
112. Tan W, Zhang D, Zhu D (2007) 4-N-Methyl-N-(2-dihydroxyboryl-benzyl) amino benzonitrile and its boronate analogue sensing saccharides and fluoride ion. Bioorg Med Chem Lett 17(9):2629–2633

113. Fülöp A, Arian D, Lysenko A, Mokhir A (2009) A simple method for monitoring protein–DNA interactions. Bioorg Med Chem Lett 19(11):3104–3107
114. Albers E, Muller BW (1995) Cyclodextrin derivatives in pharmaceutics. Crit Rev Ther Drug Carrier Syst 12(4):311–337
115. Al-Hassan KA, Khanfer MF (1998) Fluorescence probes for cyclodextrin interiors. J Fluoresc 8(2):139–152
116. Kim YH, Cho DW, Yoon M, Kim D (1996) Observation of hydrogen-bonding effects on twisted intramolecular charge transfer of p-(N, N-diethylamino) benzoic acid in aqueous cyclodextrin solutions. J Phys Chem 100(39):15670–15676
117. Panja S, Chakravorti S (2002) Photophysics of 4-(N, N-dimethylamino)cinnamaldehyde/alpha-cyclodextrin inclusion complex. Spectrochim Acta A Mol Biomol Spectrosc 58(1):113–122
118. Wang J, Nakamura A, Hamasaki K, Ikeda H, Ikeda T, Ueno A (1996) A fluorescent molecule-recognition sensor with a protein as an environmental factor. Chem Lett 4:303–304
119. Shinitzky M (1984) Membrane fluidity and cellular functions. In: Shinitzky M (ed) Physiology of membrane fluidity. CRC, Boca Raton, FL, pp 1–51
120. Nadiv O, Shinitzky M, Manu H, Hecht D, Roberts CT Jr, LeRoith D, Zick Y (1994) Elevated protein tyrosine phosphatase activity and increased membrane viscosity are associated with impaired activation of the insulin receptor kinase in old rats. Biochem J 298(Pt 2):443–450
121. Osterode W, Holler C, Ulberth F (1996) Nutritional antioxidants, red cell membrane fluidity and blood viscosity in type 1 (insulin dependent) diabetes mellitus. Diabet Med 13(12):1044–1050
122. Zubenko GS, Kopp U, Seto T, Firestone LL (1999) Platelet membrane fluidity individuals at risk for Alzheimer's disease: a comparison of results from fluorescence spectroscopy and electron spin resonance spectroscopy. Psychopharmacology (Berl) 145(2):175–180
123. Shiraishi K, Matsuzaki S, Ishida H, Nakazawa H (1993) Impaired erythrocyte deformability and membrane fluidity in alcoholic liver disease: participation in disturbed hepatic microcirculation. Alcohol Alcohol Suppl 1A:59–64
124. Maczek C, Bock G, Jurgens G, Schonitzer D, Dietrich H, Wick G (1998) Environmental influence on age-related changes of human lymphocyte membrane viscosity using severe combined immunodeficiency mice as an in vivo model. Exp Gerontol 33(5):485–498
125. Möller W, Takenaka S, Rust M, Stahlhofen W, Heyer J (1997) Probing mechanical properties of living cells by magnetopneumography. J Aerosol Med 10(3):171–186
126. Butler JP, Kelly SM (1998) A model for cytoplasmic rheology consistent with magnetic twisting cytometry. Biorheology 35(3):193–209
127. Valberg PA, Albertini DF (1985) Cytoplasmic motions, rheology, and structure probed by a novel magnetic particle method. J Cell Biol 101(1):130–140
128. Humphry-Baker R, Grätzel M, Steiger R (1980) Drastic fluorescence enhancement and photochemical stabilization of cyanine dyes through micellar systems. J Am Chem Soc 102(2):847–848
129. Haidekker M, Brady T, Wen K, Okada C, Stevens H, Snell J, Frangos J, Theodorakis E (2002) Phospholipid-bound molecular rotors: synthesis and characterization. Bioorg Med Chem 10(11):3627–3636
130. Nipper ME, Majd S, Mayer M, Lee JC, Theodorakis EA, Haidekker MA (2008) Characterization of changes in the viscosity of lipid membranes with the molecular rotor FCVJ. Biochim Biophys Acta 1778(4):1148–1153
131. Barbu VD (1991) Isoprenylation of proteins: what is its role? C R Seances Soc Biol Fil 185(5):278–289
132. Kohl NE, Conner MW, Gibbs JB, Graham SL, Hartman GD, Oliff A (1995) Development of inhibitors of protein farnesylation as potential chemotherapeutic agents. J Cell Biochem Suppl 22:145–150
133. Härtel S, Tykhonova S, Haas M, Diehl HA (2002) The susceptibility of non-UV fluorescent membrane dyes to dynamical properties of lipid membranes. J Fluoresc 12(3):465–479

134. Luby-Phelps K, Mujumdar S, Mujumdar RB, Ernst LA, Galbraith W, Waggoner AS (1993) A novel fluorescence ratiometric method confirms the low solvent viscosity of the cytoplasm. Biophys J 65(1):236–242
135. Kuimova MK, Yahioglu G, Levitt JA, Suhling K (2008) Molecular rotor measures viscosity of live cells via fluorescence lifetime imaging. J Am Chem Soc 130(21):6672–6673
136. Lodish HF (2008) Molecular cell biology, 6th edn. W.H. Freeman, New York
137. Dustin P (1984) Structure and Chemistry of microtubules. In: Microtubules, Springer-Verlag, New York, 19–94
138. Iio T, Takahashi S, Sawada S (1993) Fluorescent molecular rotors binding to actin. J Biochem 113:196–199
139. Sawada S, Iio T, Hayashi Y, Takahashi S (1992) Fluorescent rotors and their applications to the study of G–F transformation of actin. Anal Biochem 204:110–117
140. Kung CE, Reed JK (1989) Fluorescent molecular rotors: a new class of probes for tubulin structure and assembly. Biochemistry 28:6678–6686
141. Grinvald A, Fine A, Farber IC, Hildesheim R (1983) Fluorescence monitoring of electrical responses from small neurons and their processes. Biophys J 42(2):195–198
142. Ephardt H, Fromherz P (1989) Fluorescence and photoisomerization of an amphiphilic aminostilbazolium dye as controlled by the sensitivity of radiationless deactivation to polarity and viscosity. J Phys Chem 93(22):7717–7725
143. Jones MA, Bohn PW (2001) Total internal reflection fluorescence and electrocapillary investigations of adsorption at the water–dichloroethane electrochemical interface. 2. Fluorescence-detected linear dichroism investigation of adsorption-driven reorientation of di-N-butylaminonaphthylethenylpyridiniumpropylsulfonate. J Phys Chem B 105(11):2197–2204
144. Sutharsan J, Lichlyter D, Wright NE, Dakanali M, Haidekker MA, Theodorakis EA (2010) Molecular rotors: synthesis and evaluation as viscosity sensors. Tetrahedron 66:2582–2588
145. Lichlyter D, Haidekker MA (2009) Immobilization techniques for molecular rotors – towards a solid-state viscosity sensor platform. Sens Actuators B Chem 139:648–656